Preston Tube Calibration

Prepared by:
C. I. Thornton, A. L. Cox, and P.Sclafani

July 2008

Colorado State University
Engineering Research Center
Fort Collins, Colorado

Colorado State University

Preston Tube Calibration

Prepared by:
C. I. Thornton, A. L. Cox, and P.Sclafani

July 2008

Colorado State University
Engineering Research Center
Fort Collins, Colorado

Table of Contents

List of Tables

List of Figures

1 INTRODUCTION

Erosion control countermeasures in riverine environments are typically designed to maintain or stabilize some geometric aspect of the channel cross section. Countermeasures must be able to withstand forces exerted on them by the flow of water during some design event. For a successful design, engineers must have some information regarding the maximum force a specific countermeasure can withstand. Prediction of these forces requires either historical data or information collected from a physical model. Shear stress near the bed acting in the direction of flow is commonly used as a design parameter for selecting and sizing countermeasures.

Direct measurement of the bed shear stress is not straightforward and in most cases not practical. Preston (1954) suggested a linear relationship between the velocity at the boundary and the bed shear stress. Using a pitot-static tube to measure the velocity head near the bed, an indirect procedure was proposed to compute the boundary shear stress. Use of a pitot-static tube, or Preston tube, to measure boundary shear stress requires that a relationship between the boundary shear stress and velocity near the boundary be calibrated under similar conditions.

Calibration of the Preston tube requires collecting velocity data near the bed in a channel with known boundary shear stress. Preston (1954) suggested that once a relationship between shear stress and near boundary velocity under idealized conditions is developed, it can then be applied in a more general sense, to channels of similar

characteristics. This report summarizes a calibration process performed in support of physical tests being performed by Colorado State University for the Bureau of Reclamation on the Middle Rio Grande River.

The Preston tube provides a convenient method for obtaining shear stress measurements at various locations along the cross section in a physical model. Calibration of the Preston tube presented in this report specifically supports a model of the Middle Rio Grande, constructed in 2001, for the Bureau of Reclamation. The Middle Rio Grande is a 29-mile reach of the Rio Grande River in central New Mexico that extends from downstream of Cochiti Dam to Bernalillo, New Mexico. Figure 1.1 presents a map of the Middle Rio Grande reach.

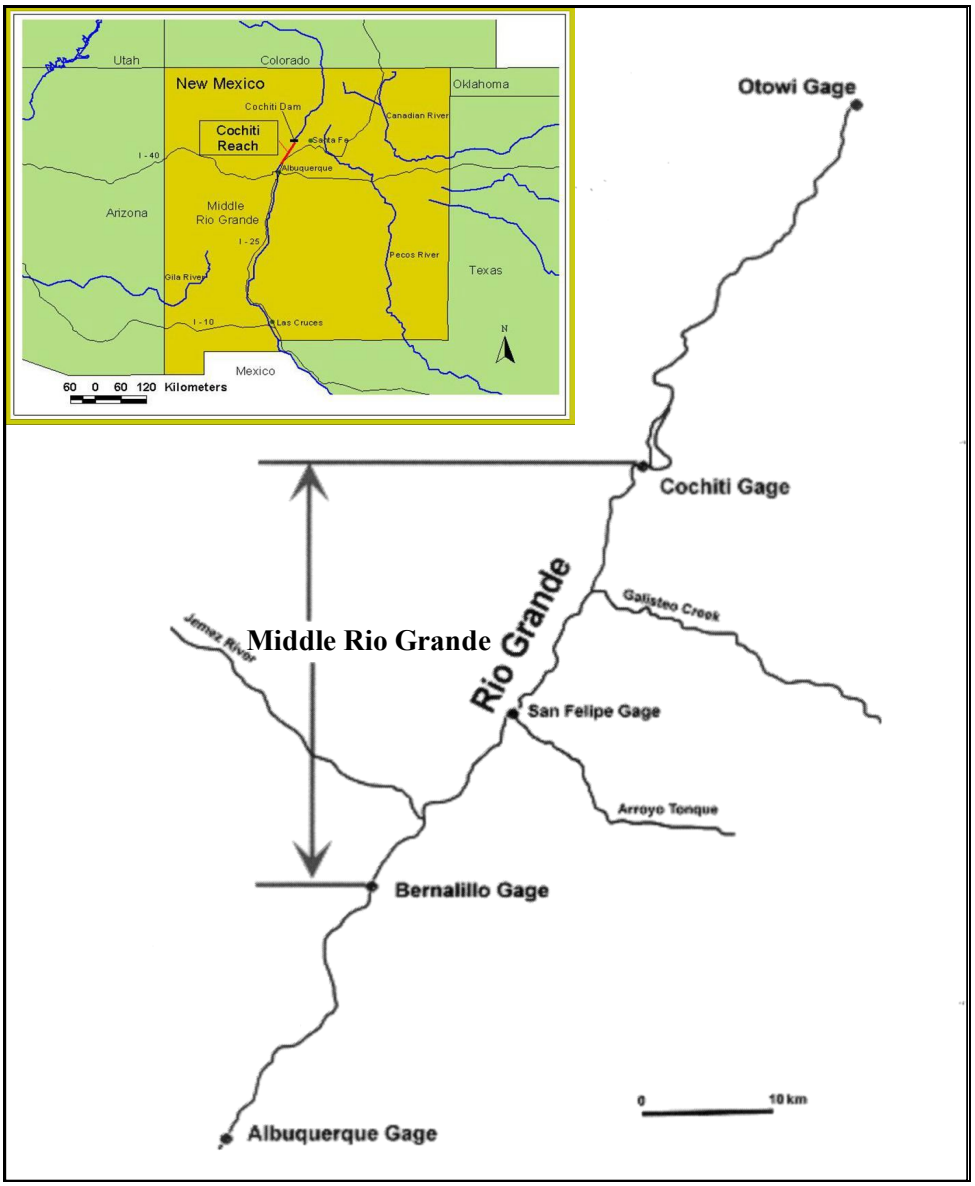

Figure 1.1: Location Map of Middle Rio Grande (Schmidt, 2005)

Degradation and instability in the Middle Rio Grande has caused the U.S. Bureau of Reclamation to investigate installation of possible stabilization countermeasures. The Middle Rio Grande provides habitat to rare and endangered species and, as a result, the Bureau of Reclamation needs to design countermeasures that stabilize the channel cross section while preserving natural habitat. Bendway weirs have been identified as

appropriate structures to potentially protect the natural habitat and protect the vulnerable river banks. Exhaustive design guidelines do not exist for these weirs, and because of the infrequency of their use, their impact is not entirely known. As a result Colorado State University has been tasked to perform a series of studies to evaluate the hydraulic effects of bendway weir installation.

A research program utilizing the rigid boundary model examined various design parameters of bendway weirs. These studies have been performed by Colorado State personnel beginning in 2001. Calibration of the Preston tube included in this report supports these studies.

2 LITERATURE REVIEW

2.1 INTRODUCTION

At the onset of the Preston tube calibration, a review of prior research provided insight for the design of testing procedures. Literature was researched as it related to the use of the pitot-static tube to measure the boundary shear stress, or skin friction. Cited research dates back to the early 1950's where skin friction was determined for a smooth copper pipe. Further research extended the use of the pitot-static tube to rough boundaries and non-prismatic cross sections.

A brief presentation of fundamental hydraulic principles also provides insight to the analytical procedures used in the Preston tube calibration. Presentation of analytical fundamentals is limited only to relevant information and is not intended to be a thorough treatment of hydraulic principles.

2.2 ANALYTICAL FUNDAMENTALS

2.2.1 BACKWATER

Computation of the water surface profiles involves finding the change in total head over some distance, dx. Total head consists of velocity head, pressure head, and elevation head as shown in Figure 2.1.

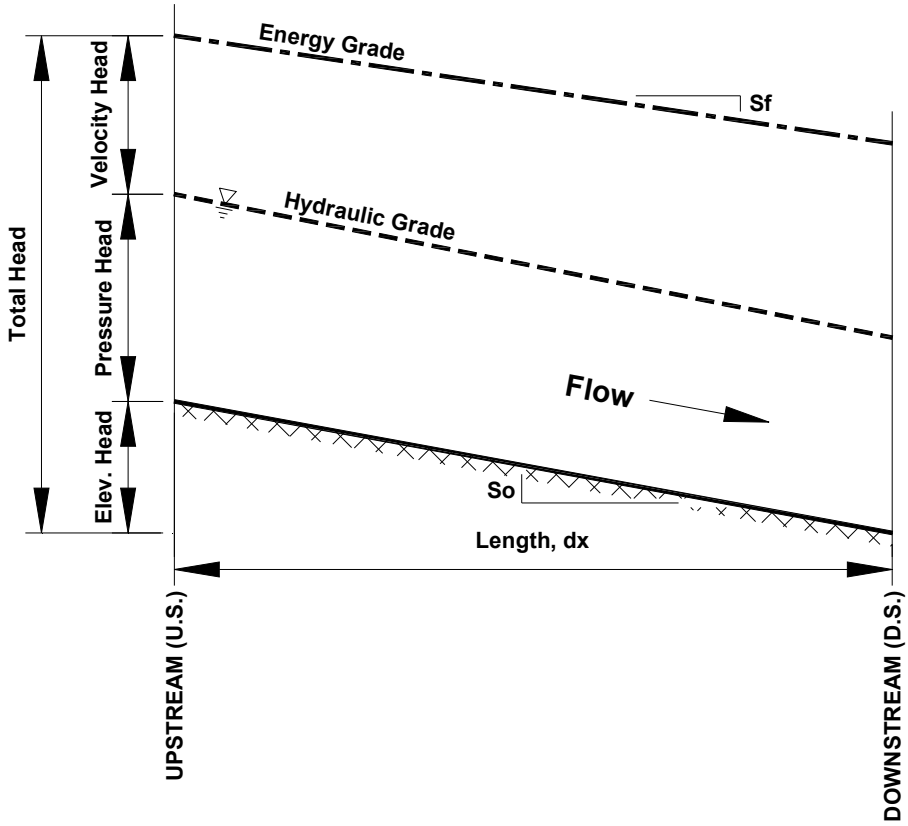

Figure 2.1: Water surface profile and components thereof.

Total head can be further defined, mathematically, as shown in Equation 2.1.

$$H = \frac{P}{\gamma} + z + \frac{V^2}{2g} \qquad \textbf{Equation 2.1}$$

where,

$H =$ total head (ft);

$\frac{P}{\gamma} =$ pressure head (ft);

$z =$ elevation head (ft);

$\frac{V^2}{2g}$ = velocity head (ft);

γ = specific weight of water (lb/ft^3); and

g = gravitational constant (ft/s^2).

Differentiating Equation 2.1 with respect to x and rearranging, results in Equation 2.2.

$$\frac{\partial}{\partial x}\left(\frac{P}{\gamma}+\frac{V^2}{2g}\right)=\frac{\partial H}{\partial x}-\frac{\partial z}{\partial x} \qquad \textbf{Equation 2.2}$$

where,

H = total head (ft);

$\frac{P}{\gamma}$ = pressure head (ft);

z = elevation head (ft);

$\frac{V^2}{2g}$ = velocity head (ft);

γ = specific weight of water (lb/ft^3); and

g = gravitational constant (m/s^2).

Substituting the bed slope, S_o, for $\partial z/\partial x$ and the friction slope, S_f, for $\partial H/\partial x$ results in the backwater Equation 2.3, which can be used to compute the change in water surface elevation over some distance, ∂x.

$$\frac{\partial}{\partial x}\left(\frac{P}{\gamma}+\frac{V^2}{2g}\right)=S_0-S_f \qquad \textbf{Equation 2.3}$$

where,

$\frac{P}{\gamma}$ = pressure head (ft);

$\frac{V^2}{2g}$ = velocity head (ft);

$S_0 = -\left(\partial z / \partial x\right)$ = bed slope;

$S_f = -\left(\partial H / \partial x\right)$ = friction slope;

γ = specific weight of water (lb/ft^3); and

g = gravitational constant (m/s^2).

Numerical solutions for Equation 2.3 include both the direct and standard step methods as presented by Chow (1959). Computation of water surface profiles for research contained in this report utilized the standard step method, where the friction slope is computed by Equation 2.4.

$$S_f = \frac{n^2 V^2}{2.22 R^{4/3}} \qquad \textbf{Equation 2.4}$$

where,

S_f = friction slope;

n = Manning's roughness coefficient;

V = cross sectional averaged flow velocity (ft/s);

$R = \frac{A}{P}$ = hydraulic radius (ft);

A = cross sectional area (ft^2); and

P = wetted perimeter (ft).

Exact matches between computed water surface profiles and known water surface profiles are not typically expected. For this reason, error associated between the computed profile and the known profile must be computed for each computational interval. One method for establishing the quality of fit is by summing the square differences between computed and known depth at each cross section. Adjustment of the computational model parameters can then be made to optimize the fit. In the case of backwater computations in the laboratory setting, where the discharge and cross sectional areas are well established, Manning's roughness and the starting water surface elevation are the primary parameters that can be adjusted to improve fit. As with any computational model, parameters that are calibrated to match expected results must still maintain a realistic sense of what the parameter is measuring. Realistic limits must be set on the degree at which these parameters can be adjusted.

2.2.2 BOUNDARY SHEAR

Boundary shear stress can be computed from a known water surface profile using fundamental principles of momentum conservation. Applying Newton's second law of motion to open channel flow systems, one can state "that the change of momentum per

unit time in the body of water in a flowing channel is equal to the resultant of all the external forces that are acting on the body" (Chow, 1959). Practical use Newtons second law involves setting momentum flux through a control volume, as defined by the change in momentum (mass times velocity) per unit time, equal to the sum of the external forces acting upon that control volume. In defining the momentum flux through a typical control volume, it is convenient to assume a constant cross sectional geometry, constant discharge, constant water density, and gradually varied flow depth over the length, L, of the control volume. Equation 2.5 gives an expression of the momentum flux through a typical control volume with a width, b; depth, y; and length, L.

$$\dot{M} = \frac{\partial mV}{\partial t} = \Delta(\rho QV) = \rho Q(V_{DS} - V_{US}) = \rho q^2 b\left(\frac{1}{y_{DS}} - \frac{1}{y_{US}}\right) \qquad \textbf{Equation 2.5}$$

where;

$\dot{M}$ = momentum flux (slug*ft/s^2);

m = mass of water within control volume (slug);

V = cross sectional averaged velocity (ft/s);

V_{US} = cross sectional averaged velocity at the upstream boundary (ft/s);

V_{DS} = cross sectional averaged velocity at the downstream boundary (ft/s);

ρ = mass density of water (assumed constant) (slug/ft^3);

Q = discharge (ft^3/s); and

$q = \frac{Q}{b}$ = discharge per unit width of channel (ft^2/s).

Considering the typical control volume of some length, L, shown in Figure 2.2, four forces can be defined to be acting on the control volume; pressure acting on the upstream and downstream faces, weight of the fluid within the control volume, and the friction force acting opposite the flow direction.

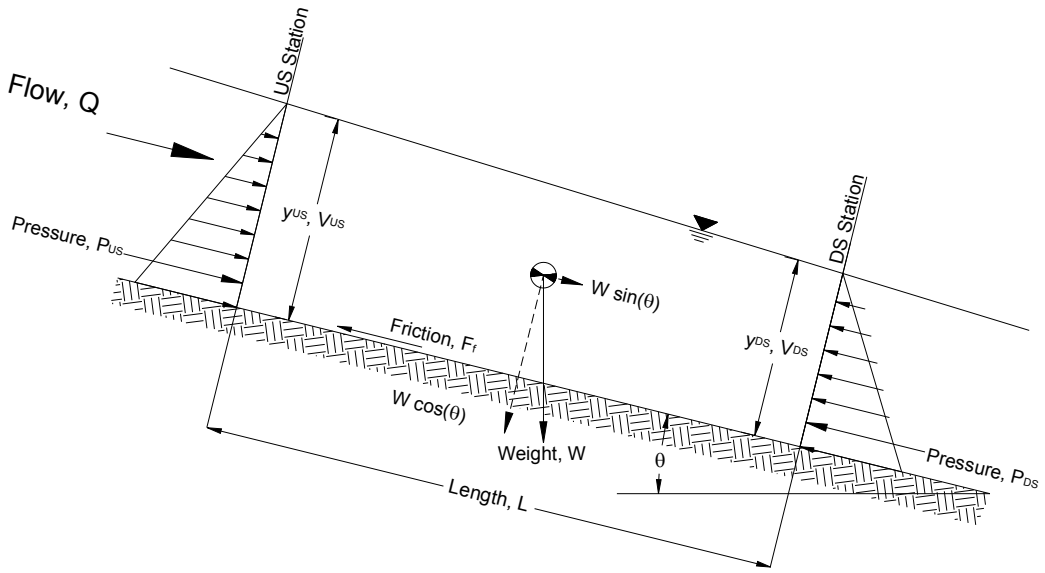

Figure 2.2: Forces acting on a typical open channel flow control volume.

From Figure 2.2 an expression, summing these four forces, can be created.

$$\Sigma F_x = P_{US} - P_{DS} + W\sin(\theta) - F_f \qquad \textbf{Equation 2.6}$$

where;

ΣF_x = Sum of the forces in the principle (x) direction of flow (slug*ft/s^2);

P_{US} = pressure exerted on the upstream face of the control volume (slug*ft/s^2);

P_{DS} = pressure exerted on the downstream face of the control volume (slug*ft/s^2);

W = weight of the fluid within the control volume (slug*ft/s^2);

θ = angle of the bed slope; and

F_f = friction force acting on the bed surface (slug*ft/s^2).

Development of an expression for boundary shear stress in a rectangular channel can proceed by considering each one of the terms listed in Equation 2.6. If the flow depth across the control volume is gradually varied, and hydrostatic conditions persist, then the pressure can be expressed as a function of depth, shown in Equation 2.7.

$$P = \left[\frac{1}{2}(\gamma y) y b\right]\cos\theta \qquad \textbf{Equation 2.7}$$

where;

P = pressure (slug*ft/s^2);

y = flow depth (ft);

b = channel width (ft);

γ = specific weight of water (lb/ft^3); and

θ = bed slope angle.

Applying Equation 2.7 to upstream and downstream faces of the control volume results in Equation 2.8, an expression for the total depth as a function of depth.

$$P_T = P_{US} - P_{DS} = \frac{1}{2}\gamma b\left(y_{US}^2 - y_{DS}^2\right)\cos\theta \qquad \textbf{Equation 2.8}$$

where;

P_T = total pressure (slug*ft/s^2);

P_{US} = pressure at downstream face of control volume (slug*ft/s^2);

P_{DS} = pressure at upstream face of control volume (slug*ft/s^2);

y_{US} = upstream flow depth (ft);

y_{DS} = downstream flow depth (ft);

b = channel width (ft);

γ = specific weight of water (lb/ft^3); and

θ = bed slope angle.

Weight of the fluid within the control volume can be computed by multiplying the specific weight of water by the volume of the fluid within the control volume. Volume of the control volume can be expressed, for a rectangular channel, as a function of a constant width, average depth, and length, shown in Equation 2.9.

$$W = \gamma V = \gamma\left(b\bar{y}L\right) = \gamma bL\frac{\left(y_{US} + y_{DS}\right)}{2} \qquad \textbf{Equation 2.9}$$

where;

W = weight of water within the control volume (slug*ft/s^2);

V = volume of water within the control volume (ft^3);

b = channel width (ft);

L = length of control volume (ft);

$\bar{y}$ = average flow depth over control volume length (ft);

y_{US} = upstream flow depth (ft);

y_{DS} = downstream flow depth (ft);

γ = specific weight of water (lb/ft^3);

Friction force can be computed by the multiplication of the shear stress by the area of the surface that is in contact with the water. For a rectangular flume with plexiglass sides, the frictional force created by the bed is much greater then that created by the sides. Thus, the wetted perimeter for a rectangular plexiglass channel with a rough bed can be assumed to be the channel width. Equation 2.10 shows the equation for friction force within a typical control volume.

$$F_f = \tau_o A = \tau_o (P_w L) = \tau_o (bL) \qquad \textbf{Equation 2.10}$$

where;

F_f = friction force ($slug*ft/s^2$);

τ_o = boundary shear stress ($slug/ft*s^2$);

A = cross sectional area (ft^2);

P_w = wetted perimeter (ft);

L = length of control volume (ft); and

b = channel width (ft).

Equation 2.11 shows the result of combining Equation 2.8, Equation 2.9, and Equation 2.10.

$$\Sigma F_x = P_{US} - P_{DS} + W\sin\theta - F_f$$

$$\Sigma F_x = \frac{1}{2}\gamma b\left(y_{US}^2 - y_{DS}^2\right)\cos\theta + \gamma bL\frac{\left(y_{US} + y_{DS}\right)}{2}\sin\theta + \tau_o\left(bL\right) \qquad \textbf{Equation 2.11}$$

where;

ΣF_x = sum of the forces in the downstream (x) direction (slug*ft/s^2);

P_{US} = pressure at the upstream face of the control volume (slug*ft/s^2);

P_{DS} = pressure at the downstream face of the control volume (slug*ft/s^2);

W = weight of the fluid within the control volume (slug*ft/s^2);

F_f = friction force (slug*ft/s^2);

b = width of channel (ft);

L = length of control volume (ft);

y_{US} = upstream flow depth (ft);

y_{DS} = downstream flow depth (ft);

τ_o = boundary shear stress (slug/ft*s^2); and

θ = bed slope angle.

A final expression for the boundary shear stress can be derived from solving Equation 2.11 for the boundary shear stress, τ_o, and simplifying. This final expression is shown in Equation 2.12.

$$\tau_o = \frac{1}{2}\gamma\left(y_{US} + y_{DS}\right)\sin\theta + \frac{1}{L}\left[\frac{1}{2}\gamma\left(y_{US}^2 - y_{DS}^2\right)\cos\theta + \rho q^2\left(\frac{1}{y_{DS}} = \frac{1}{y_{US}}\right)\right] \quad \textbf{Equation 2.12}$$

where;

τ_o = boundary shear stress (slug/ft*s^2);

y_{US} = upstream flow depth (ft);

y_{DS} = downstream flow depth (ft);

L = length of control volume (ft);

q = unit discharge (ft^2/s);

θ = bed slope angle;

γ = specific weight of water (lb/ft^3); and

ρ = mass density of water (slug/ft^3).

It can also be shown that the boundary shear stress can be approximated from Equation 2.13. Equation 2.12 and Equation 2.13 differ only by a $\cos\theta$.

$$\tau_o = \gamma R S_f \qquad \textbf{Equation 2.13}$$

where;

τ_o = boundary shear stress (slug*ft/s^2);

R = hydraulic radius (equal to the average depth across the control volume) (ft);

S_f = energy slope; and

γ = specific weight of water (lb/ft^3).

2.2.3 PITOT-STATIC TUBE

Pitot-static tubes are used to measure velocity in a moving stream. Function of the pitot-static tube is based on Bernoulli's principle which states that for an incompressible, inviscid flow along a stream line the sum of the static head, dynamic head, and elevation head remains constant (Munson, 1994). Bernoulli's principal can be applied to two points shown Figure 2.3 where point 1 is located within fully developed 1-dimensional flow, undisturbed by the pitot-static tube and point 2 is located at a point very close to the pitot-static tube.

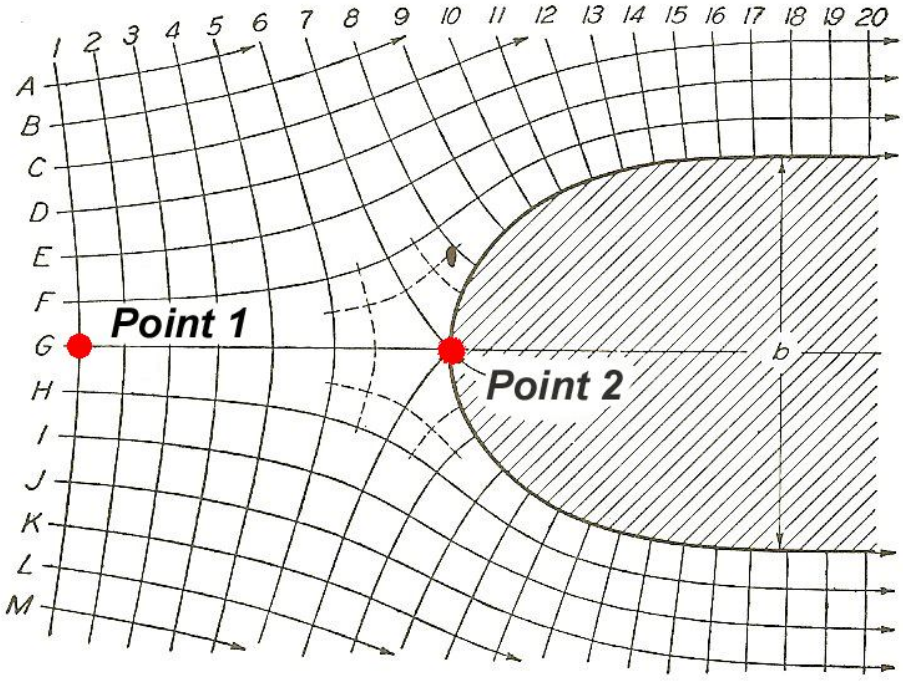

Figure 2.3: Flow approaching an object such as the pitot-static tube (Rouse, 1978).

As a fluid approaches the opening of the total pressure port of a pitot-static tube, the velocity reduces to zero; this is the point of stagnation. Because the streamlines cannot go through solid objects, they must bend around the opening, causing a point of zero velocity very close to the opening. According to Bernoulli's principle the total head at point 1 in Figure 2.3 must equal the total head at point 2, as expressed in Equation 2.14.

$$\frac{p_1}{\gamma} + \frac{V_1^2}{2g} = \frac{p_2}{\gamma} \qquad \textbf{Equation 2.14}$$

where;

p_1 = pressure at point 1 (slug*ft/s^2);

p_2 = pressure at point 2 (slug*ft/s^2);

V_1 = velocity at point 1 (ft/s);

g = gravitation acceleration (ft/s^2); and

γ = specific weight of water (lb/ft^3).

Because the velocity at the pitot-static tube opening is zero, the head measured by the pitot tube is the total head. Figure 2.4 shows the components of a typical pitot-static tube.

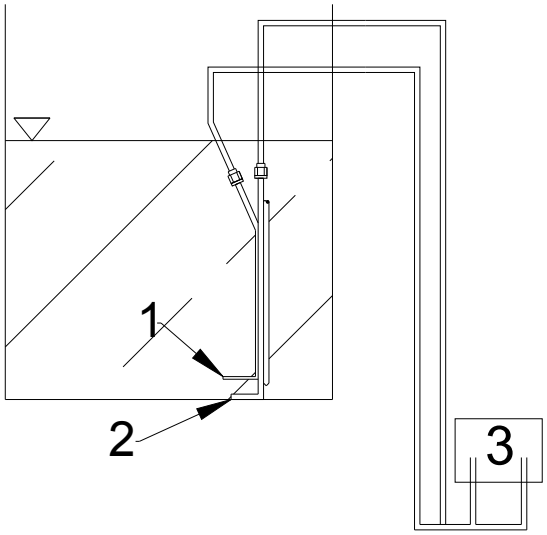

1. Total pressure port on pitot-static tube.
2. Static pressure port on pitot-static tube.
3. High and low pressure connections on pressure transducer.

Figure 2.4: Schematic of typical pitot-static tube.

Point 2 in Figure 2.4 measures the total pressure experienced at the stagnation point. Point 1 measures the static pressure within the normal flow field. Dynamic head can be computed by subtracting the static head at point 1 from the total head at point 2, similar

to Equation 2.14. The pitot-static tube, therefore, can be used to determine the velocity at any point within a uniform flow field.

2.3 SUMMARY OF RELAVANT RESEARCH

2.3.1 LUDWIEG AND TILLMANN (1950)

Ludwieg and Tillmann (1950) presented results of research that used a method of determining the shear stress by measuring the amount of heat transfer from small element embedded in the surface of the wall. From boundary layer theory, the velocity profile next to the wall, in the fully turbulent zone, can be expressed as shown in Equation 2.15.

$$\frac{u}{U_*} = a \log\left(\frac{U_* y}{\nu}\right) + b \qquad \textbf{Equation 2.15}$$

where,

a and b = universal constants;

u = velocity a distance y from the boundary (ft/s);

U_* = shear velocity (ft/s); and

ν = kinematic viscosity of water (ft^2/s).

Approximation of the velocity profile can be made using a power law, as presented in Equation 2.16.

$$\frac{u}{U_*} = C\left(\frac{U_* y}{\nu}\right)^{1/n} \qquad \textbf{Equation 2.16}$$

where,

C and n = constants that depend on $\frac{U_* y}{\nu}$

u = velocity a distance y from the boundary (ft/s);

U_* = shear velocity (ft/s); and

ν = kinematic viscosity of water (ft^2/s).

Figure 2.5 shows results from tests performed by Ludwieg and Tillman (1950) for various flow conditions on a horizontal plate.

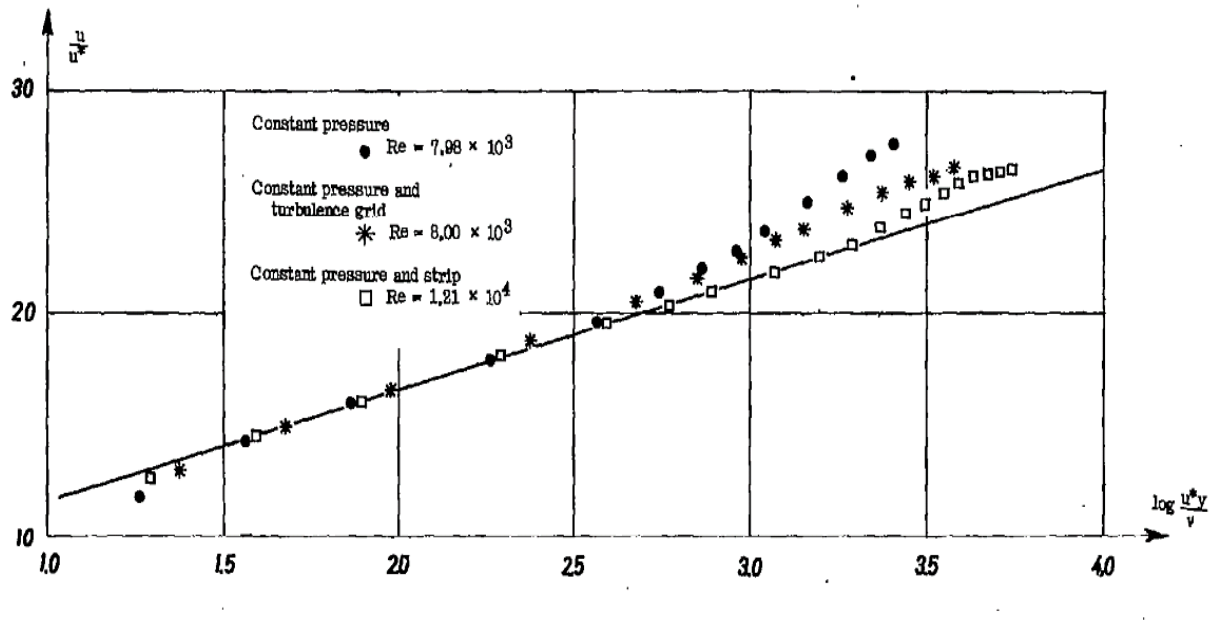

Figure 2.5: Velocity profiles from selected tests with the universal law plotted as a solid line (Ludwieg and Tillmann, 1950).

Within the limits of the Ludwieg and Tillmann (1950) tests, Figure 2.5 shows reasonable evidence in support of Equation 2.15 and Equation 2.16.

2.3.2 PRESTON (1954)

The purpose of this investigation was to develop a simple method to deduce the skin friction that could be applied to surfaces in motion through air and water as well as physical laboratory models. Skin friction is a function of the velocity and the shear stress near the wall (Equation 2.17).

$$c_f = \frac{\tau_o}{\frac{1}{2}\rho u^2} \qquad \textbf{Equation 2.17}$$

where,

c_f = skin friction coefficient;

τ_o = boundary shear stress (slug*ft/s^2);

ρ = mass density of water (slug/ft^3); and

u = velocity near boundary (ft/s).

Therefore, estimation of the skin friction requires an estimate of both the shear stress and velocity near the boundary. Using a pitot-static tube, the velocity near the bed can be determined by measuring the difference between the static and dynamic pressure. Further, substituting the relationship for shear velocity, presented in Equation 2.18, into Equation 2.16 from Ludwieg and Tillman (1950), a modified relationship can be deduced as shown in Equation 2.19.

$$U_*^2 = \frac{\tau_o}{\rho} \qquad \textbf{Equation 2.18}$$

where,

U_* = shear velocity (ft/s);

τ_o = shear stress (slug*ft/s^2); and

ρ = mass density of water (slug/ft^3).

$$\frac{(P - p_o)d^2}{\rho\nu^2} = F\left(\frac{\tau_o d^2}{\rho\nu^2}\right) \qquad \textbf{Equation 2.19}$$

where,

F = representative linear function;

P = dynamic pressure (slug*ft/s^2);

p_o = static pressure (slug*ft/s^2);

d = pitot tube diameter taken as a representative length (ft);

ρ = mass density of water (slug/ft^3);

ν = kinematic viscosity of water (ft^2/s); and

τ_o = boundary shear stress (slug*ft/s^2).

To determine the function, *F*, in Equation 2.19, calibration is required in a section of known boundary shear. In a circular pipe the boundary shear can be directly computed using Equation 2.20

$$\tau_o = (p_1 - p_2)\frac{D}{4L} \qquad \textbf{Equation 2.20}$$

where,

τ_o = boundary shear stress (slug*ft/s^2);

p_1 = pressure at the beginning of length, L (slug*ft/s^2);

p_2 = pressure at the end of length, L (slug*ft/s^2);

D = internal diameter of pipe (ft); and

L = test section (ft).

Four pitot tubes were used during Preston (1954) experimentation, corresponding to four tube diameters shown in Table 2.1.

Table 2.1: Diameters of pitot tubes used in Preston (1954) research.

Pitot Tube Number	**1**	**2**	**3**	**4**
External Diameter (in.)	0.02915	0.0544	0.0907	0.1214
Ratio: (Internal/External) Diameter	0.602	0.603	0.599	0.598

Static pressures were measured from 0.02 inch diameter taps located at seven (7) inches, ten (10) inches, and sixteen (16) inches from the down stream end of the test section for p_o, p_2, and p_1, respectively. Tests were performed in a 23-foot section of 2-inch internal diameter brass pipe with a polished smooth inner wall. Approximately 14 feet preceded the test section (89 pipe diameters). A schematic of the testing apparatus is shown in Figure 2.6.

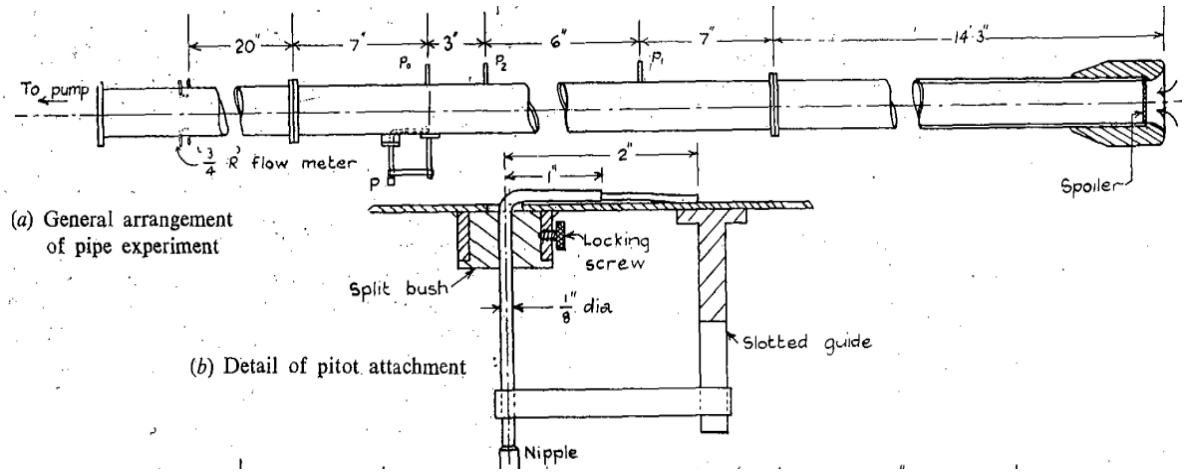

Figure 2.6: Schematic of test section from Preston (1954)

During testing, the velocity within the pipe was varied to achieve a range of Reynolds number of 10^4 to 10^5 for all four pitot tubes shown in Table 2.1. The results of these tests are shown in Figure 2.7.

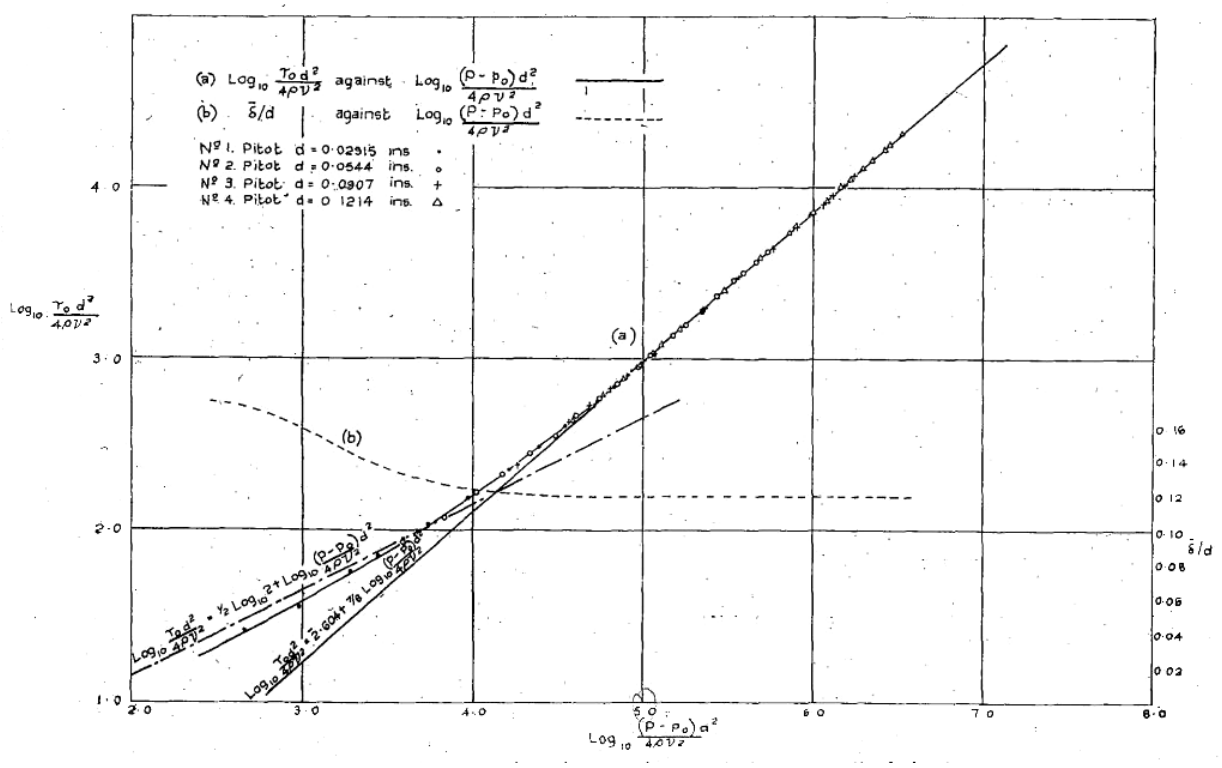

Figure 2.7: Results from Preston (1954)

Equation 2.21 shows a regression line fit to the data shown in Figure 2.5.

$$\log_{10}\left(\frac{\tau_o d^2}{4\rho\nu^2}\right) = -1.396 + \frac{7}{8}\log_{10}\left[\frac{(P - p_o)d^2}{4\rho\nu^2}\right] \qquad \textbf{Equation 2.21}$$

where,

P = dynamic pressure (slug*ft/s^2);

p_o = static pressure (slug*ft/s^2);

d = pitot tube diameter taken as a representative length (ft);

ρ = mass density of water (slug/ft^3);

ν = kinematic viscosity of water (ft^2/s); and

τ_o = boundary shear stress (slug*ft/s^2).

Using known values for the properties of water and the pitot tube diameters presented in Table 2.1, Equation 2.21 can be reduced to a calibration equation for each size tube as shown in Table 2.2.

RECHECK MATH BEFORE FINALIZING OR TAKE OUT !!!!!****

Table 2.2: Calibrated equations based on tested pitot tubes (Preston, 1954)

Pitot Tube Number	Inside Diameter (in)	Calibrated Equation τ_o [psf]; ΔH [in]
1	0.0175	$\tau_o = 0.0644(\Delta H)^{7/8}$
2	0.0328	$\tau_o = 0.0551(\Delta H)^{7/8}$

3	0.0543	$\tau_o = 0.0486(\Delta H)^{7/8}$
4	0.0726	$\tau_o = 0.0452(\Delta H)^{7/8}$

From Figure 2.7 the regression line is supported by experimental data only for a range of $\log_{10}\left[\frac{(P-p_o)d^2}{4\rho\nu^2}\right]$ between approximately 4.5 and 6.5.

Additional tests were performed using round pitot tubes in a wind tunnel and a flat pitot tubes in the pipe. Traverses were made in both environments to determine the velocity profiles. Figure 2.8 shows a non-dimensional plot of the pitot traverses.

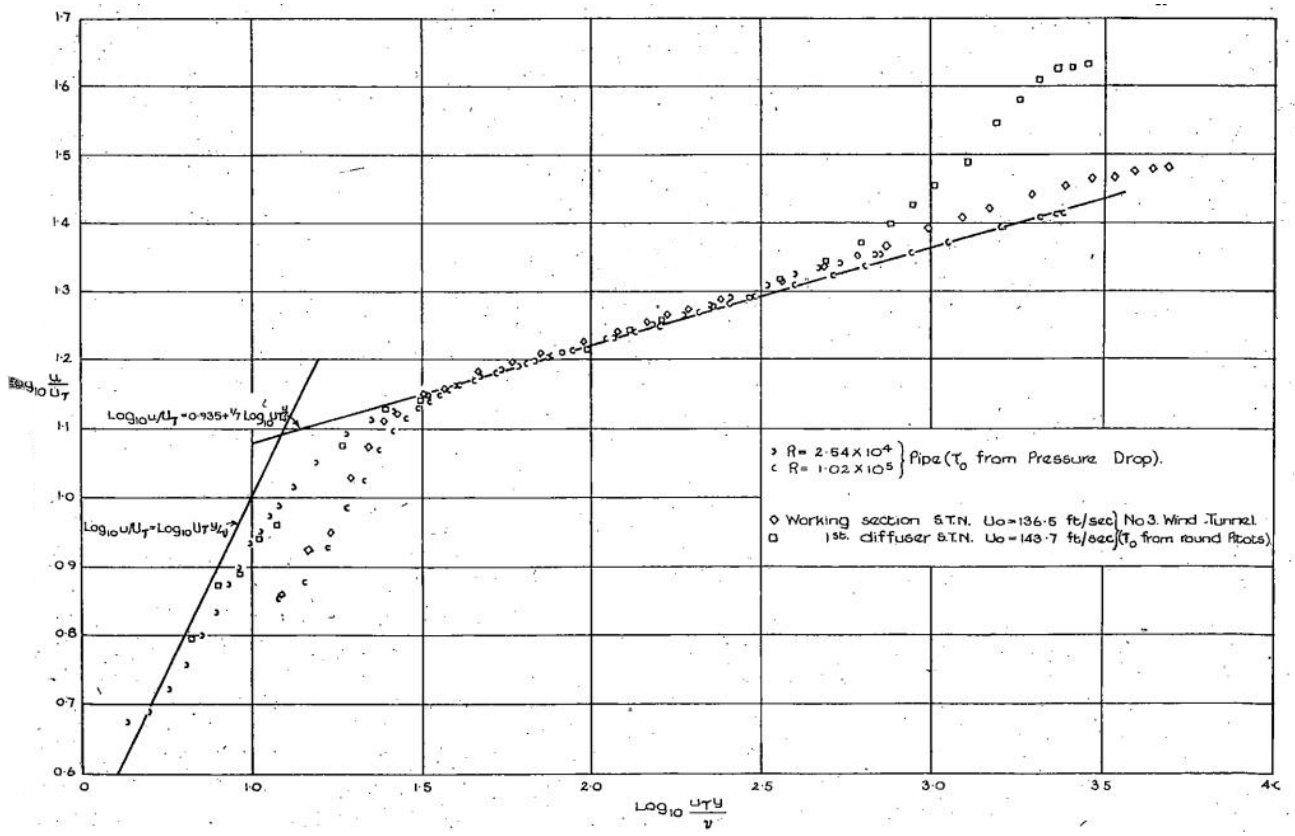

Figure 2.8: Observation from pitot traverses (Preston, 1954)

Regression through the plotted data indicated that the velocity profiles could be sufficiently described by a 1/7 power law when $\log\left(\frac{U_* y}{\nu}\right)$ is in the range of approximately 1.5 to 2.75. Equation 2.22 shows the resulting power relationship.

$$\frac{u}{U_*} = 8.61\left(\frac{U_* y}{\nu}\right)^{1/7} \qquad \textbf{Equation 2.22}$$

where,

u = velocity a distance y from the boundary (ft/s);

U_* = shear velocity (ft/s); and

ν = kinematic viscosity of water (ft^2/s).

2.3.3 HSU (1955)

One contribution to previous research by Preston (1954) was to develop, empirically, an equation to compute shear stress from a pitot-static tube reading. Hsu (1955) develops a theoretical form of Equation 2.21 for smooth boundaries. A theoretical relationship between shear and pressure was developed by computing the total pressure acting on the tube; integrating over the area of tube opening. Equation 2.23 is obtained from performing this integration in the turbulent boundary layer, assuming that the velocity profile may be expressed as a $1/7^{th}$ Power law (Preston, 1954).

$$\log_{10}\left(\frac{\tau_o d^2}{4\rho\nu^2}\right) = \log k + \frac{7}{8}\log_{10}\left[\frac{(P - p_o)d^2}{4\rho\nu^2}\right] \qquad \textbf{Equation 2.23}$$

where,

P = dynamic pressure (slug*ft/s^2);

p_o = static pressure (slug*ft/s^2);

d = pitot tube diameter taken as a representative length (ft);

ρ = mass density of water (slug/ft^3);

ν = kinematic viscosity of water (ft^2/s);

τ_o = boundary shear stress (slug/ft*s^2); and

$\log k$ = calibration constant.

Experiments run in a wind tunnel with a 1/16-inch pitot tubes demonstrated agreement with Equation 2.21. Data from Hsu (1955) were compared to the Preston (1954) calibration equation; but no new relationship was determined.

2.3.4 IPPEN AND DRINKER (1960)

As part of a larger study of shear stress distributions of bends in an open channel, Ippen and Drinker (1960) sought to generally apply the methodology presented by Preston (1954) to both straight and curved free surface flow. To justify use of the pitot-static tube (Preston tube) to free surface flow, six (6) velocity profiles near the boundary were recorded using a pitot tube at various locations along the bend and in the straight channel. From these velocity profiles, the shear velocity, U_*, was computed from the boundary shear stress. Boundary shear stress was computed by using Preston's 1954 calibration, Equation 2.21. Figure 2.9 shows the collected data plotted with the empirically derived equation of the velocity profile presented in Equation 2.22 (Preston,

1954). Agreement, shown in Figure 2.9, between the empirical equations for the velocity profile and the collected data provide supporting evidence to the validity of using Preston's 1954 calibrated equation, Equation 2.21, to compute the shear stress in free surface flow for smooth walled flumes with both straight and curved sections.

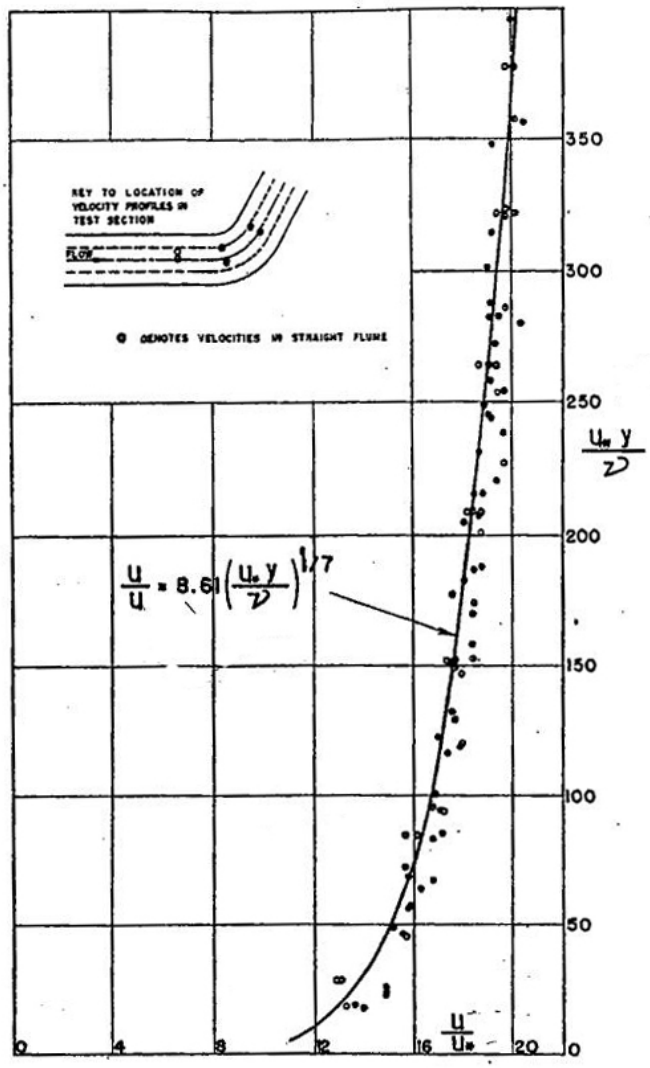

Figure 2.9: Velocity distribution in free surface flow with a smooth boundary (Ippen and Drinker, 1960)

A 0.432-inch diameter pitot-static tube was then calibrated to measure boundary shear stress for free surface flow with rough boundaries. Within a straight flume, a 20-

foot section of rough surface was installed. A 6-foot section near the downstream end was used for the test reach. Preston tube measurements were taken and plotted against the shear stress, which was computed as shown in Equation 2.24.

$$\tau_o = \gamma\, y_o S_e \qquad \textbf{Equation 2.24}$$

where,

τ_o = boundary shear stress (slug/ft*s^2);

γ = specific weight of water (slug/ft^2*s);

y_o = depth from the surface to the bottom of the roughness particles (ft); and

S_e = energy slope.

Derivation of the turbulent shear relation for fully rough flow required including the roughness element height in the integration of pressure over the depth of the pitot tube dynamic port. This integration revealed that $\tau_o \propto (\Delta p)$ rather than $\tau_o \propto (\Delta p)^{7/8}$. Regression of the collected data resulted in the relationship shown in Equation 2.25, where ΔH is in ft. For ΔH in inches, the coefficient of 1.30 would change to 0.1083.

$$\tau_o = 1.30\Delta H \qquad \textbf{Equation 2.25}$$

where,

τ_o = boundary shear stress (psf); and

ΔH = preston tube reading (ft);

2.3.5 HEINZ (2000)

Calibration of the Preston tube by Heinz (2000), was based on the Ippen and Drinker's (1960) paper involving use of the Preston tube on rough boundary. Ippen and Drinker's equation, presented in Equation 2.25 having a coefficient of 1.30, can be expressed in general as shown in

$$\tau_o = C\Delta H \qquad \textbf{Equation 2.26}$$

where,

C = calibration coefficient;

τ_o = boundary shear stress (psf); and

ΔH = preston tube reading (ft).

A comparison was made between Preston tube measurements taken in the centerline of the constructed channel and shear stress computed as $\gamma y S_e$. Heinz (2002) prepared a computer model, using the Corps of Engineer's HEC-RAS computer software, simulating baseline conditions (with no obstructions in the channel). Within the HEC-RAS model of baseline conditions, the roughness coefficient was adjusted to minimize the sum of the square error between the computed profile and the measured profile collected during testing. Minimizing the error between computed and measured profiles resulted in a Manning's roughness coefficient of 0.017. Plotting the computed shear stress as a function of the Preston tube reading, and fitting a trendline through the data resulted in the calibrated Equation 2.27.

$$\tau_o = 1.7397\Delta H$$ **Equation 2.27**

where,

C = calibration coefficient;

τ_o = boundary shear stress (psf); and

ΔH = preston tube reading (ft).

2.3.6 PRESTON TUBE CALIBRATION IN THE 8-INCH FLUME

Heinz calibrated the Preston tube by collecting data in the center of the trapezoidal channel for three different discharges over the entire length of the Rio Grande model. To eliminate effects of curvature and potential lack of uniform flow development, a second calibration was performed by CSU in a rectangular 8-inch wide, 1-foot 4-inch tall, and 32 feet long plexiglass flume; shown in Figure 2.10.

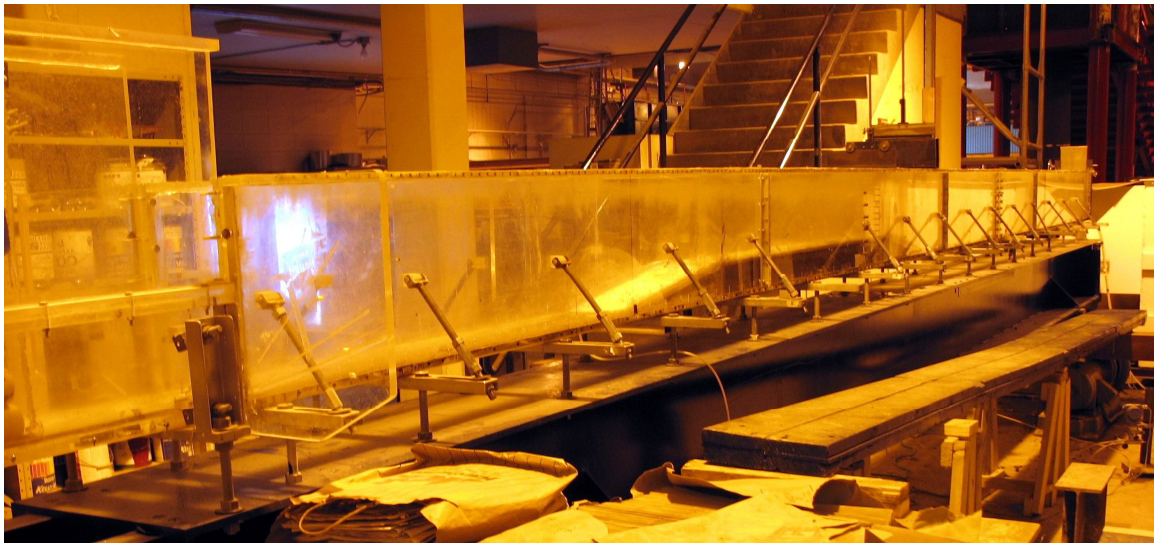

Figure 2.10: 8-inch wide by 1-foot 4-inch tall by 32 feet long plexiglass flume.

To distribute the flow before entering the test section a diffuser made up of a series of 4-inch long PVC pipes was placed at the upstream end of the flume as shown in Figure 2.11. The design of the PVC pipes was intended to both distribute the flow across the cross section and to orientate the flowlines in the downstream direction, thus, help ensure fully develop flow in the flume.

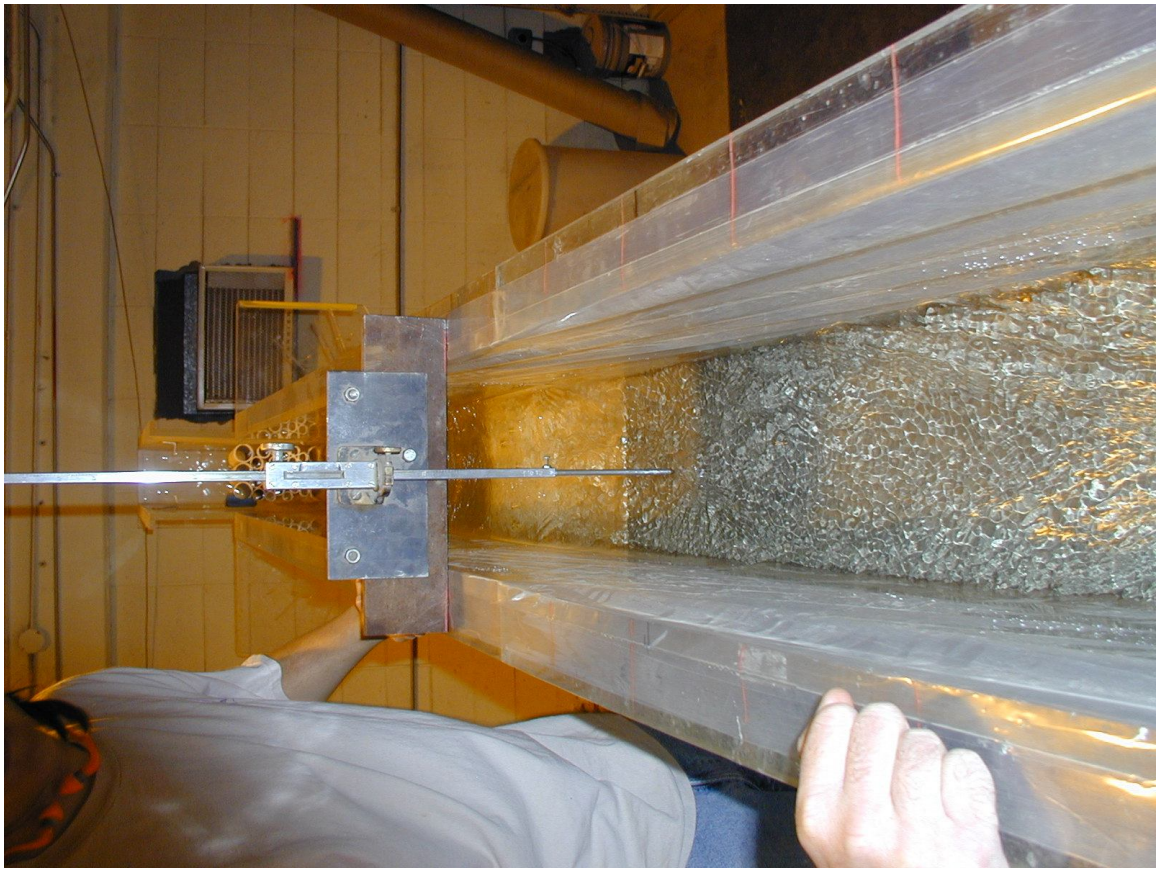

Figure 2.11: Diffuser used in the 8-inch flume.

A 6-foot long test section was placed 6-foot 11 inches from the upstream entrance of the flume. The test section for the 8-inch flume was constructed of a 4-inch thick layer of concrete placed on the plexiglass flume floor. Two 2-foot long wood transitions were constructed at either end of the test section to transition back to the existing flume floor. Figure 2.12 shows a profile schematic of the flume used for the 8-inch calibration.

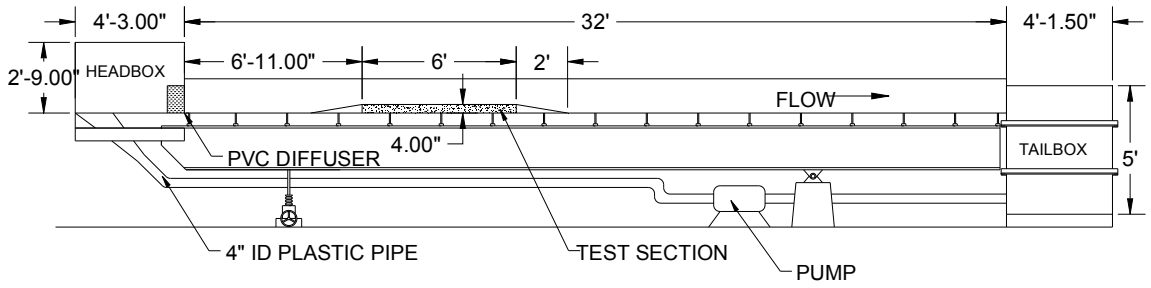

Figure 2.12: Profile schematic of the Preston tube calibration in the 8-inch flume.

The texture of the test section can be characterized as unbrushed, leveled concrete. Any surface roughness within the test section of the 8-inch flume was a result of the gravel substrate used in the concrete mix. Figure 2.13 shows a close up view of the surface texture of the test section in the 8-inch flume.

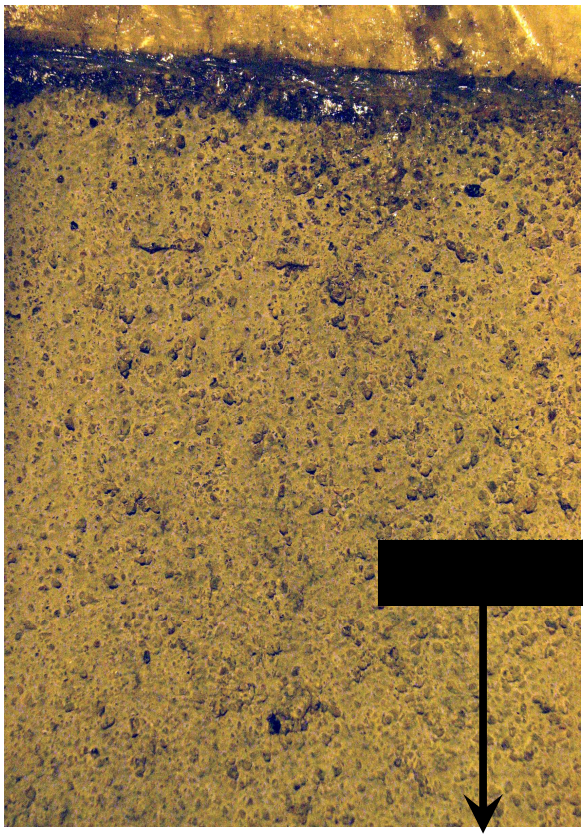

Figure 2.13: Surface texture in the test section of the 8-inch flume.

Data collection for each test included 13 data collection locations within the test section. At these locations, depth of water was measured and Preston tube readings were recorded. Data point locations are illustrated in Figure 2.14.

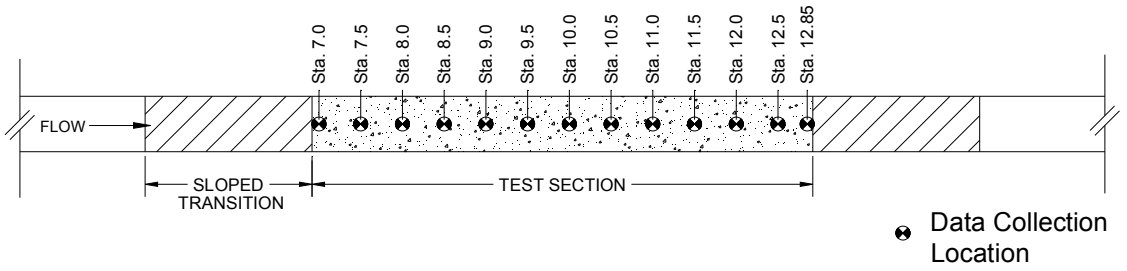

Figure 2.14: Location of data points for Preston tube calibration in 8-inch flume.

In order to achieve the range of Preston tube readings required for calibration, the slope and discharge were varied during testing. A total four slopes were tested: 0.005 ft/ft, 0.03 ft/ft, 0.04 ft/ft, and 0.05 ft/ft. For each slope, the discharge rate was varied from 0.25 cfs to 0.86 cfs. Figure 2.15 illustrates the test matrix used for the Preston tube calibration in the 8-inch flume.

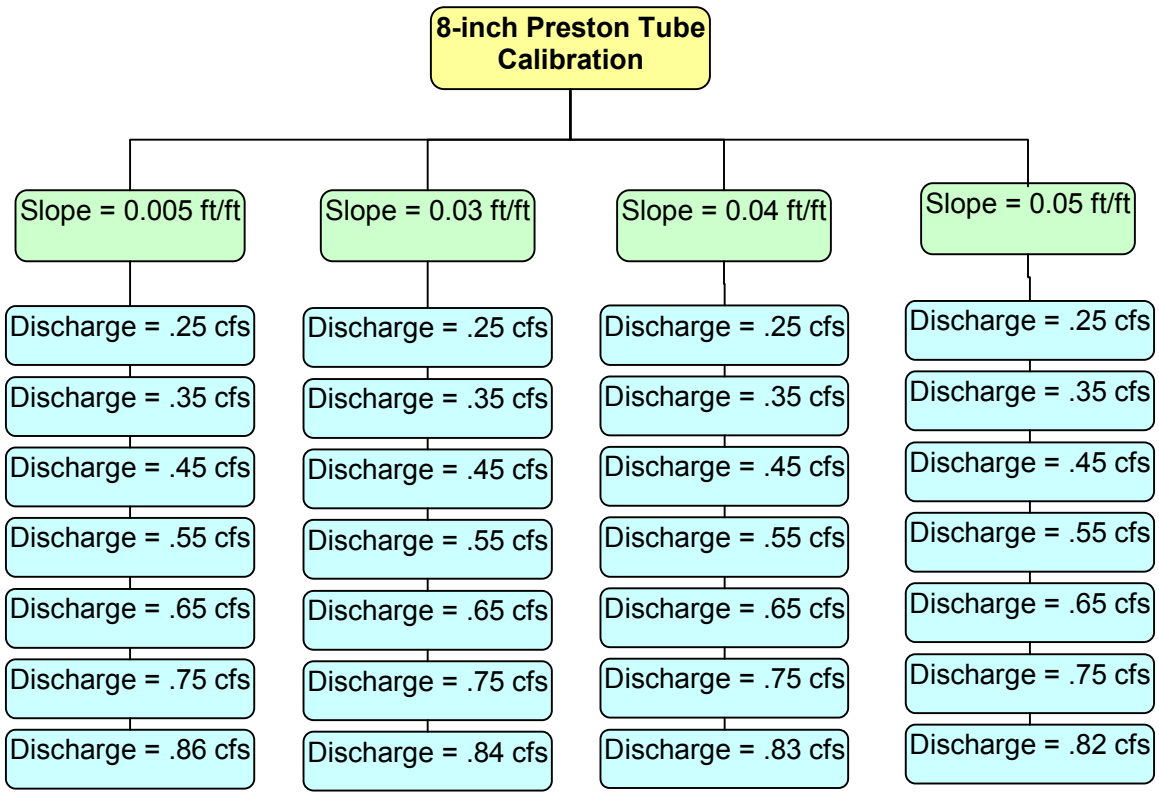

Figure 2.15: Test matrix for the Preston tube calibration in the 8-inch flume.

Calibration of the Preston tube requires corresponding a specific Preston tube reading to a known boundary shear stress. For fully developed flow in a rectangular cross section, the boundary shear stress can be computed using momentum principles and known water surface profiles. Using the full momentum equation can become computationally difficult for profiles with fluctuating depth of flow from section to section. Areas where there is an adverse water surface slope or bed slope can cause the momentum equation to give erroneous results. Reduction of these fluctuations can be accomplished by normalizing the water surface and bed profiles. Assuming an average bed slope, a water surface profile can be computed from standard backwater computational procedures with a starting water surface from measured data at the

downstream end of the test section. Comparing the computed profile and the measured profile and iterating over a range of bed roughness values until the error between the two profiles is minimized produces a normalized profile that can be used to give average boundary shear stress values. Normalization of the water surface profile using backwater computations was used during the Preston tube calibration in the 8-inch flume. Roughness values were optimized for each test. Table 2.3 summarizes the roughness coefficient values used in the Preston tube calibration in the 8-inch flume.

Table 2.3: Roughness values used in Preston tube calibration in the 8-inch flume.

Slope (ft/ft)	Discharge (cfs)	Manning's Roughness
0.005	0.25	0.028
0.005	0.35	0.029
0.005	0.45	0.032
0.005	0.55	0.032
0.005	0.65	0.032
0.005	0.75	0.033
0.005	0.86	0.034
0.030	0.25	0.024
0.030	0.35	0.026
0.030	0.45	0.026
0.030	0.55	0.027
0.030	0.65	0.029
0.030	0.75	0.030
0.030	0.84	0.030
0.040	0.25	0.023
0.040	0.35	0.025
0.040	0.45	0.026
0.040	0.55	0.027
0.040	0.65	0.029
0.040	0.75	0.030
0.040	0.83	0.031
0.050	0.25	0.025
0.050	0.35	0.025
0.050	0.45	0.027
0.050	0.55	0.029
0.050	0.65	0.029
0.050	0.75	0.029
0.050	0.82	0.029

A calibration curve can be created from the collected Preston tube data and the computed boundary shear stress. For the Preston tube calibration in the 8-inch flume, some of the data near the upstream and downstream end of test section were not used in the calibration. The stations eliminated from the regression vary with each test. Table 2.4 summarizes the upstream and downstream stations, in feet, used for calibration of the Preston tube in the 8-inch flume.

Table 2.4: Actual test section used in analysis for Preston tube calibration in the 8-inch flume.

Slope (ft/ft)	Discharge (cfs)	Beginning of Test Section used in Analysis (given as station in feet)	End of Test Section used in Analysis (given as station in feet)
0.005	0.25	9.0	12.5
0.005	0.35	9.0	12.5
0.005	0.45	9.0	12.5
0.005	0.55	9.0	12.5
0.005	0.65	9.0	12.5
0.005	0.75	9.0	12.5
0.005	0.86	9.0	12.5
0.030	0.25	9.0	11.5
0.030	0.35	9.0	12.0
0.030	0.45	9.0	12.5
0.030	0.55	9.0	12.5
0.030	0.65	9.0	12.0
0.030	0.75	9.0	12.0
0.030	0.84	9.0	12.5
0.040	0.25	9.5	12.0
0.040	0.35	9.5	12.0
0.040	0.45	9.5	12.0
0.040	0.55	9.0	12.0
0.040	0.65	9.5	12.0
0.040	0.75	9.0	12.0
0.040	0.83	9.0	12.5
0.050	0.25	9.0	11.5
0.050	0.35	9.0	11.0
0.050	0.45	9.0	12.0
0.050	0.55	9.0	12.5
0.050	0.65	9.0	12.5
0.050	0.75	9.0	12.5
0.050	0.82	9.0	12.5

Final results for the calibration of the Preston tube in the 8-inch flume are presented in Figure 2.16.

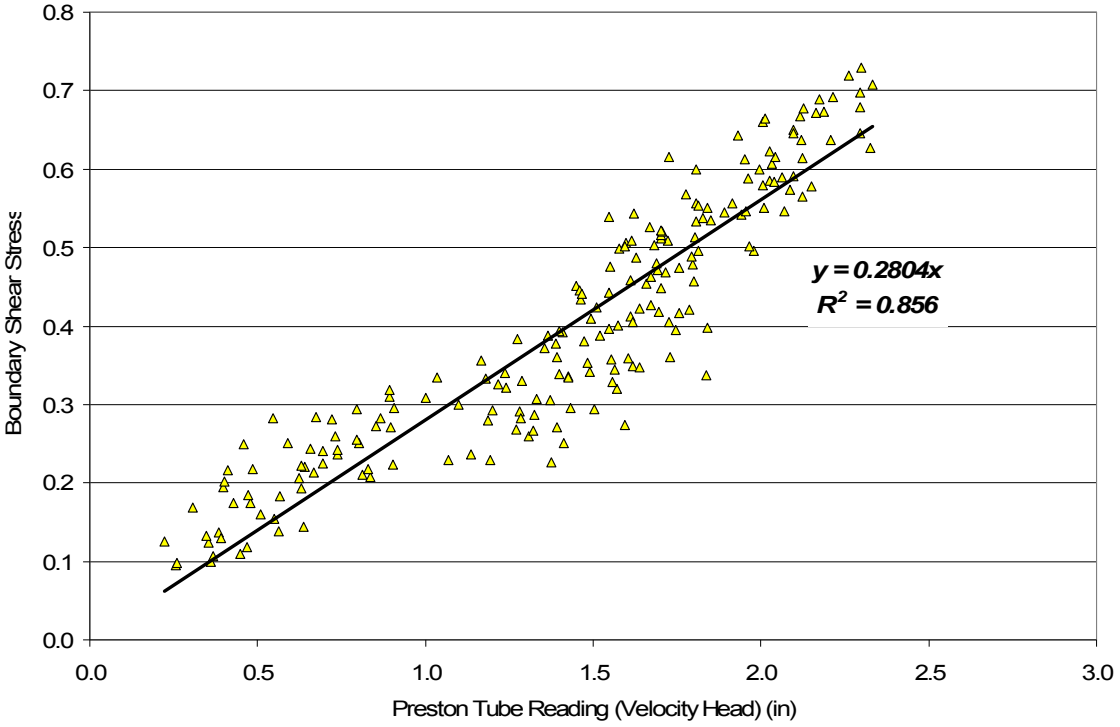

Figure 2.16: Calibration curve for the Preston tube in the 8-inch flume.

Although the regression equation appears to adequately fit the data (R^2 =.856), the spread of the data appears to be large, especially when considering a Preston tube reading of 1.5 in, where the boundary shear stresses ranges from 0.20 psf to 0.55 psf. Large variation in the boundary shear stress for a single Preston tube reading could be due to a number of factors including the flow not being fully developed, flow still converging due to short test section, or even abrupt changes in the water surface profile due to unexpected variation in the bed surface. For this reason additional testing of the Preston tube was conducted in a larger facility with a longer test section that included a more substantial approach section.

3 CONSTRUCTION

3.1 INTRODUCTION

Calibration of the Preston tube was performed in a straight 4-foot wide by approximately 2.5 feet tall by 60 feet long flume. Water is delivered to the headbox of the flume through a 6-inch and a 24-inch pipe. In the headbox, water passes through a 2.5 feet tall diffuser before entering the flume. Figure 3.1 shows a schematic of the 4-flume used for calibration of the Preston tube.

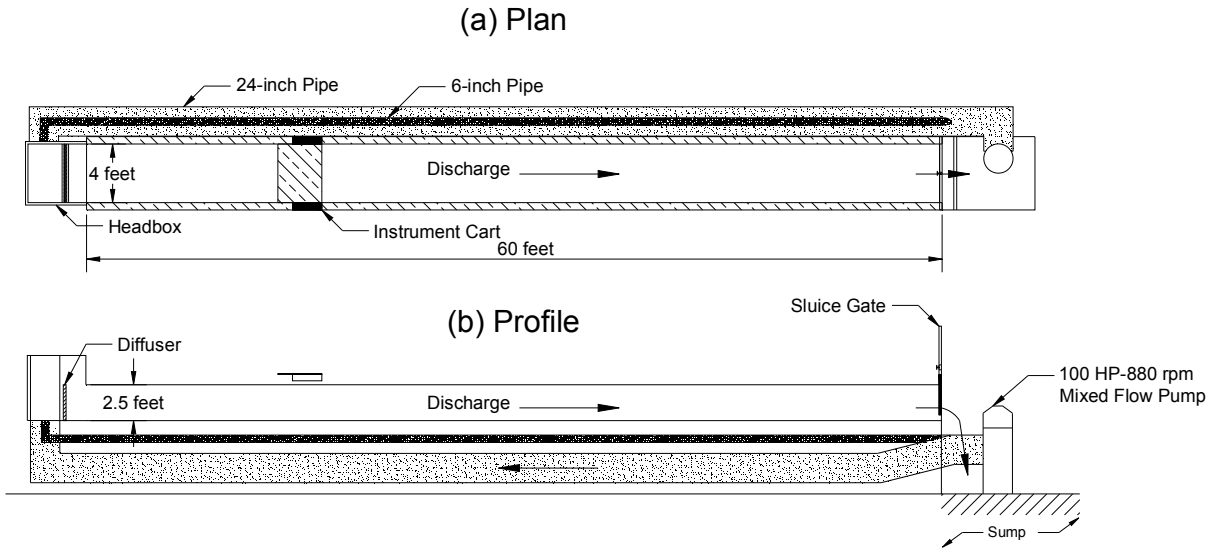

Figure 3.1: Schematic of test facility for Preston tube calibration.

A sluice gate at the downstream end of the flume controls the tailwater elevation. When the sluice gate is open, water discharges freely into the sump, approximately 5 ft below the downstream edge of the flume. A 100-Hp, 880 rpm pump provides enough

head to the pipes to deliver a maximum of approximately 22 cfs in the 24-inch line and approximately 3.5 cfs in the 6-inch line.

To date, two distinct bed surfaces have been modeled in the Middle Rio Grande study; a brushed concrete and a ¼-inch gravel bed. Preston tube readings are part of the data collected for both of these surfaces; therefore, calibration is required for each.

3.2 GRAVEL BED

On top of the existing flume bottom, approximately 2 inches of dry gravel:cement mixture was placed beginning 5 feet from the head box and extending downstream for 48 feet. A 1-foot sloped transition was formed at either end of the gravel bed, creating a 50-foot length of roughened surface. The test section used for calibration began 25 feet from the upstream end of the gravel bed and ended 4-foot from the downstream end of the gravel bed. Figure 3.2 shows the extents of the gravel bed installed in the flume.

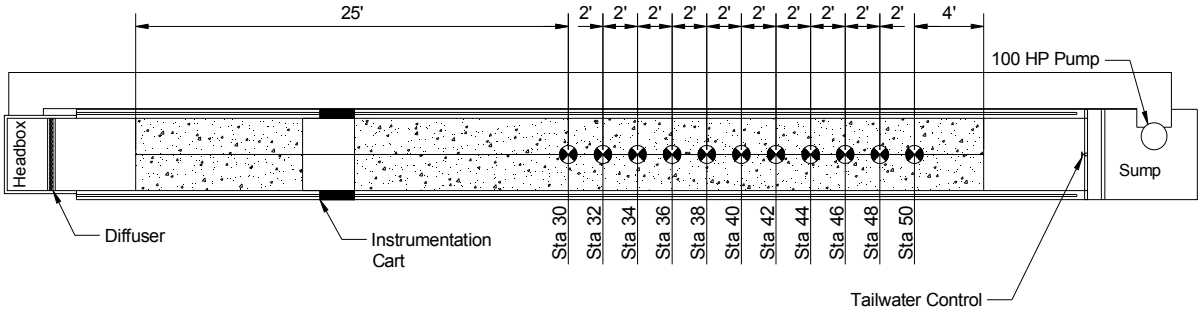

Figure 3.2: Location of gravel bed relative to the flume.

To match the gravel surface used in the native topography Rio Grande study, ¼-inch washed rock was mixed with Portland cement. A dry mixture for the gravel bed was created using approximately 5-96 lb bags of cement for each ton of gravel. A total of

approximately 3 tons of gravel were used during the construction of the gravel bed surface. The gravel mixture was brought into the flume dry, and leveled using a frame attached to the instrument cart. Bolts on either end of the cart allowed the height of the leveling frame to be appropriately adjusted for each station. Survey of the cart relative to the bed provided the appropriate height for the leveling frame. Figure 3.3 shows the process used while leveling the gravel surface.

Figure 3.3: Construction method used for the gravel surface.

Once leveled, the gravel surface was sprayed with a light mist and left to harden over 48 hours. Figure 3.4 shows the finished gravel bed relative to the Preston tube. While the dynamic port of the Preston tube is larger than the individual particles, significant roughness still exists directly in front of the tube.

Figure 3.4: Preston tube on the surface of the gravel bed in the 4-foot flume.

A survey of the hardened gravel bed provided the final slope of the test section. Figure 3.5 shows bed fluctuations around an average slope of 0.0007 ft/ft.

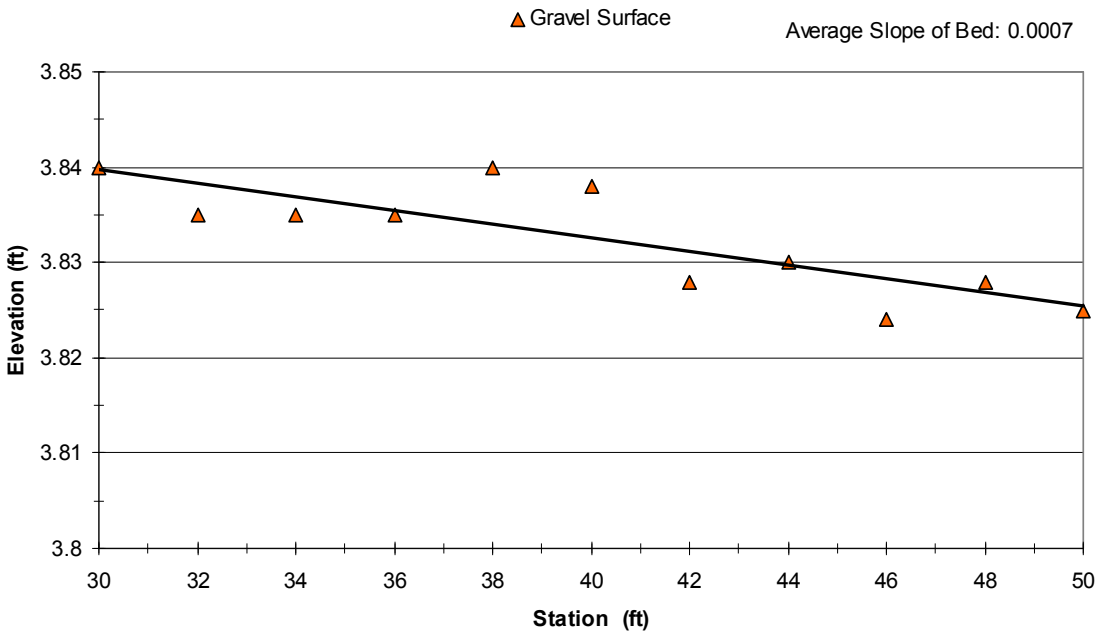

Figure 3.5: Finished gravel surface survey over the test reach.

Deviations, described as the difference between the idealized bed and the actual gravel surface, provides a comparison between the finished surveyed bed and the normalized slope of 0.0007 ft/ft. Deviations of the gravel bed surface from the idealized 0.0007 ft/ft slope are summarized in Table 3.1.

Table 3.1: Surveyed gravel surface elevation compared with normalized bed.

Station (ft)	Bed Elevation (ft)	Idealized Bed* (ft)	Difference (ft)
30	3.840	3.840	0.000
32	3.835	3.838	0.003
34	3.835	3.837	0.002
36	3.835	3.835	0.000
38	3.840	3.834	0.006
40	3.838	3.833	0.005
42	3.828	3.831	0.003

44	3.830	3.830	0.000
46	3.824	3.828	0.004
48	3.828	3.827	0.001
50	3.825	3.825	0.000
		Mean Difference:	***0.002 ft***
		Maximum Difference:	***0.006 ft***

**Note: Idealized Bed is based on a slope of 0.0007 and an intercept of 3.861 ft.*

The maximum deviation occurs at station 38 where the difference between the surveyed bed and the idealized bed is 0.006 ft. Overall, the mean of the differences between the idealized slope and the actual slope within the test reach is 0.002 ft. Although these differences are noted, they are presumed to be within acceptable limits. Locations of noted fluctuations, however, were considered during analysis of the collected data

3.3 CONCRETE CAP

When the Middle Rio Grande model was originally constructed a concrete cap was poured over a layer of sand that had been contoured to the desired cross section shape. This cap was leveled, smoothed, and brushed as shown in Figure 3.6.

Figure 3.6: Installation of the concrete cap in the Middle Rio Grande model.

While attempting to match the original surface texture of the Middle Rio Grande, three tests were constructed varying both cement:sand:gravel ratios and surface treatments. Two initial test, shown in Figure 3.7, were poured with two different cement:sand:gravel ratios: 1:2:0 and 1:3:3.

Figure 3.7: Two tests of concrete mixture for the concrete cap: Cement:Sand ratio of 1:2 (left) and Cement:Sand:Gravel ratio of 1:3:3 (right).

A 1:3:3 cement:sand:gravel mixture was determined to be too rough, and since strength of the surface was not an important criteria, including gravel in the mixture provided no particular advantage. While the cement:sand:gravel mixture of 1:2:0 resulted in a smoother surface than the 1:3:3 the resulting texture was still not satisfactory. When texturing the surface of the 1:2:0 sample, excessive downward pressure on the broom produced texture that was rougher than the surface on the Middle Rio Grande model. A third test was conducted with the 1:2:0 mixture using two different finishes, half smooth and the other half lightly brushed, using only the weight of the broom for downward pressure. Figure 3.8 shows a comparison of the first test using the 1:2:0 mixture and downward pressure (left) and the third test with the 1:2:0 mixture and half light pressure and half smoothed (right). The lower portion of Figure 3.8 shows the condition of the concrete cap in the Middle Rio Grande model. It can be seen that the light pressure best matches the surface of the Middle Rio Grande model.

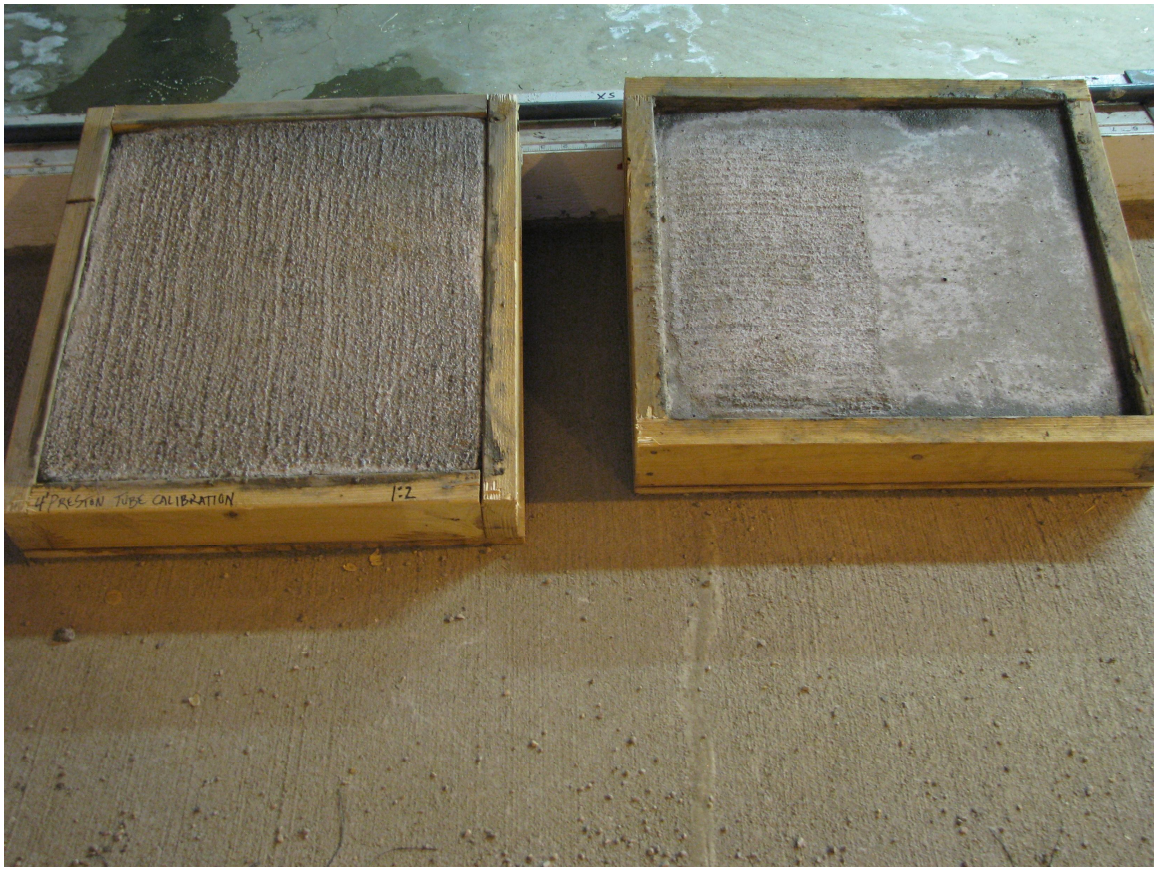

Figure 3.8: Samples of the surface texture for the 1:2:0 cement:sand:gravel mixture with downward pressure (left) and half light pressure and half smoothed texture (right).

When installing the concrete cap on top of the gravel bed, the dry 1:2:0 mixture was brought to the flume, mixed on-site, placed, and leveled to the desired depth. Masking tape, placed approximately 2 inches above the gravel bed, served as a guide for the placement of the concrete. Grease was applied to the sides of the flume to prevent the concrete from adhering to the flume. Once placed, the concrete was given 48 hours to cure before being surveyed. Figure 3.9 shows the Preston tube on the surface of the concrete cap after the concrete was cured. Comparison of Figure 3.4 with Figure 3.9 shows that the concrete cap, while containing some roughness elements, has less overall roughness with less obstructions at the face of the high pressure port of the Preston tube.

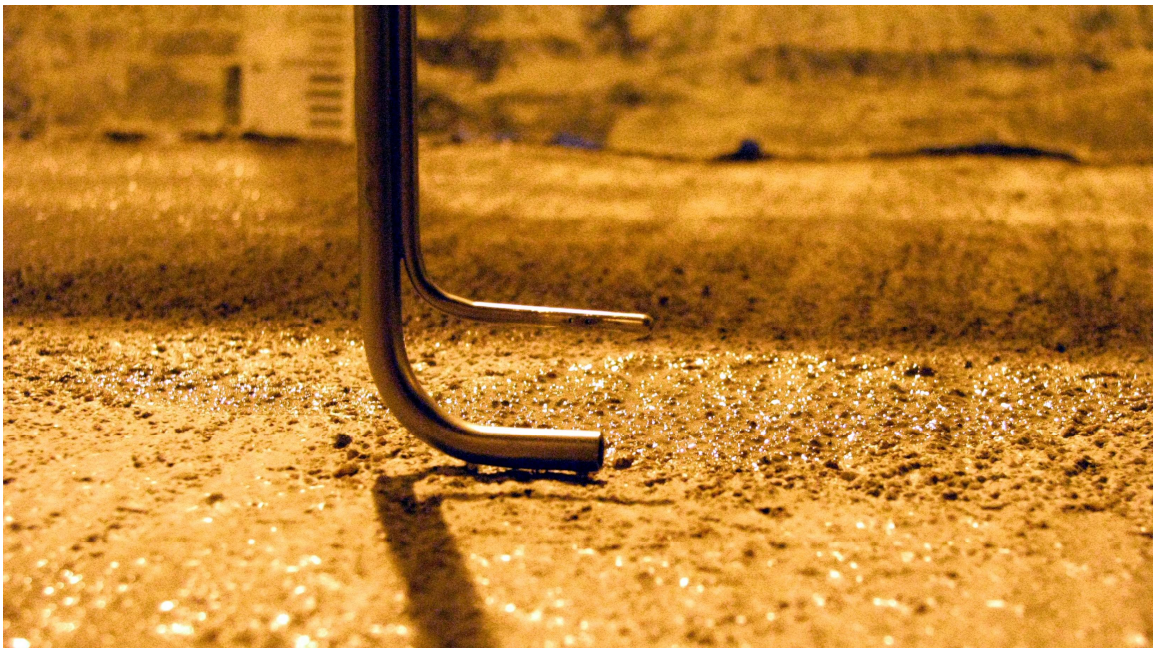

Figure 3.9: Preston tube on the surface of the concrete cap in the 4-foot flume.

Once dry, the concrete cap was surveyed to determine the finished slope. Adjustment of the flume slope was necessary to achieve the desired average slope. A second survey of the concrete cap was performed to verify the finished slope. Results of the final survey are plotted in Figure 3.10.

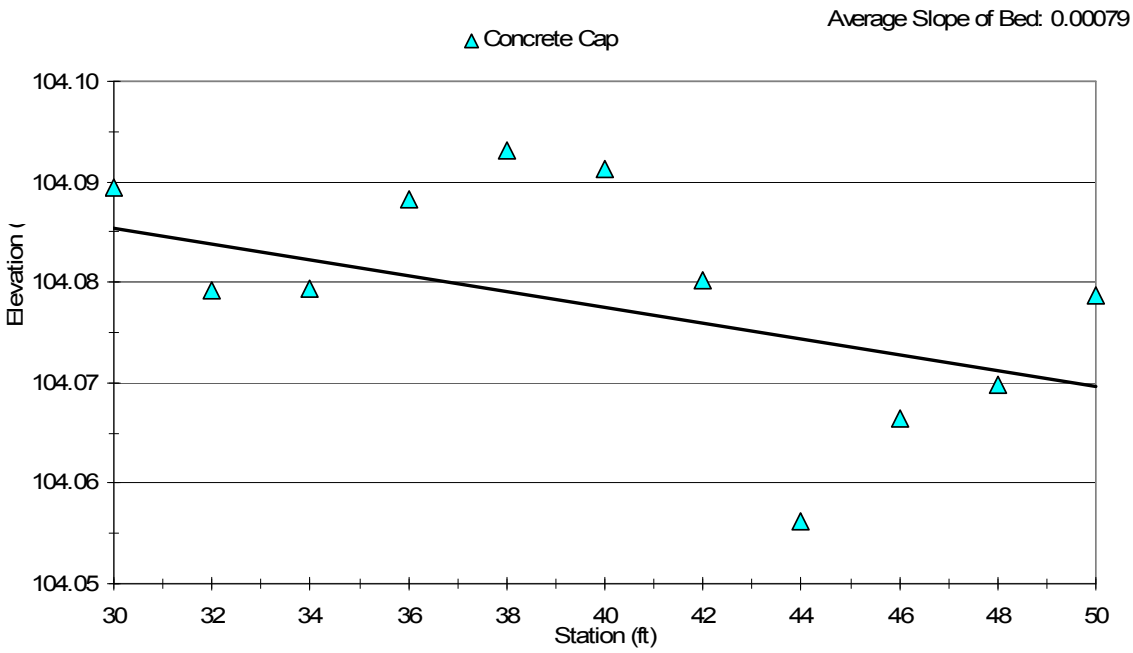

Figure 3.10: Finished concrete cap survey over the test reach.

The mean slope based on Figure 3.10 was 0.00078 ft/ft. Fluctuations between the idealized slope of 0.00078 ft/ft were computed and summarized Table 3.2.

Table 3.2: Surveyed concrete cap elevation compared with normalized cap.

Station (ft)	Bed Elevation (ft)	Idealized Bed* (ft)	Difference (ft)
30	104.089	104.089	0.001
32	104.079	104.087	0.008
34	104.079	104.085	0.006
36	104.088	104.083	0.005
38	104.093	104.081	0.012
40	104.091	104.079	0.012
42	104.080	104.077	0.003
44	104.056	104.076	0.019
46	104.067	104.074	0.007

48	104.070	104.072	0.002
50	104.079	104.070	0.009

Mean Difference: ***0.008 ft***

Maximum Difference: ***0.019 ft***

** Idealized Bed is based on a slope of 0.00078 and an intercept of 104.11 ft*

A mean difference of 0.008 ft between the actual surveyed bed and the idealized slope was computed while a maximum difference of 0.019 ft occurred at station 44. Figure 3.10 shows a .014 ft rise in the surface beginning near station 36 and then dropping again by 0.035 ft at station 44. Modifications to the concrete cap to adjust these fluctuations were considered but ultimately found to be unfeasible. Fluctuations in the bed surface occurring at stations 38 and 44 were noted and taken into account during data analysis.

3.4 UPSTREAM DISTRIBUTION OF FLOW

Two measures were taken to help distribute the flow across the cross section and eliminate turbulent fluctations; a diffuser was installed at the exit to the headbox and 3-4-foot by 4-foot scour stop mats were installed immediately after the headbox. Figure 3.11 shows the diffuser used in the headbox of the 4-foot flume.

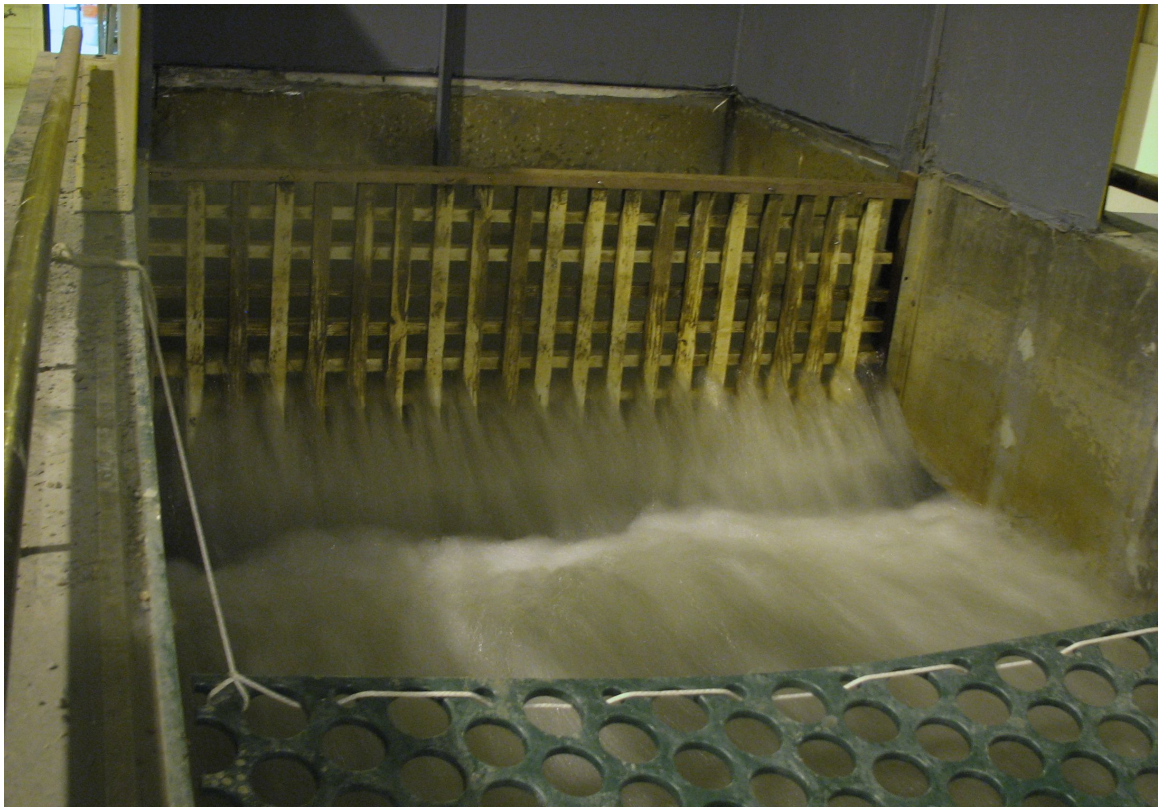

Figure 3.11: Diffuser in the headbox of the 4-foot flume.

Downstream of the diffuser three scour stop mats were installed to suppress turbulent wave fluctuations in the flume. One scour stop mat was originally installed, however, during preliminary tests, it was determined that more needed to be added. Figure 3.12 shows three scour stop mats that were added to suppress turbulent wave fluctuations.

Figure 3.12: Scour stop mats installed at the upstream end of the 4-foot flume.

4 INSTRUMENTATION

4.1 INTRODUCTION

For both the gravel bed and the concrete cap, a 20-foot section at the downstream end of the flume was isolated as a test section where depth data and Preston tube measurements were taken. A 25-foot approach section upstream of the test section helped ensure fully developed flow before the data collection points. A total of eleven points, from station 30 to station 50, are included within the test section. Figure 4.1 illustrates a schematic of the test reach with data location points identified.

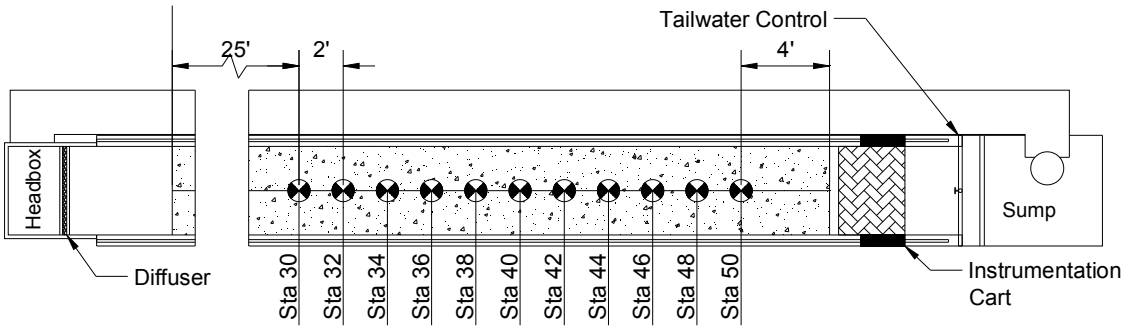

Figure 4.1: Test reach and data point locations within the 4-foot flume.

4.2 DEPTH MEASUREMENT

Depth was measured in feet using a point gage, with an accuracy of 0.001 ft, in the center of the flume for each station within the test section. A profile, normalized about the measured data, was computed from standard step backwater procedures (Chow, 1959). For the profiles with no backwater, water surfaces from measured bed and depth at the downstream section were used for downstream boundary conditions in the standard step procedure. For the profiles with backwater, boundary conditions were set equal to the average depth over the entire test section. An average bed slope computed from the surveyed data was used for the normalized slope in the backwater computations. Manning's roughness coefficients were selected based on minimizing the error between the resulting computed water surface profile and the measured water surface profile. For iterative processes within the backwater computations, the tolerance was set to 0.00001 ft.

4.3 SHEAR STRESS COMPUTATION

From the normalized water surface profiles, the shear stress was computed using momentum principles. For this procedure, the control volume of 0.2 feet was used to match the computational interval of the backwater computations. At each station, the shear stress was determined by averaging the computed shear stress over the two control volumes bounding the station. For example, at station 40, the reported shear stress was the average between the computed shear stress in the control volume from 39.8 to 40.0 and in the control volume from 40.0 to 40.2.

4.4 PRESTON TUBE MEASUREMENT

4.4.1 PRESTON TUBE CONFIGURATION

The Preston tube used for this calibration is made up of two stainless steel pipes; a larger pipe to measure the total pressure and a smaller pipe to measure the static pressure. A stainless steel housing was fabricated to attach the Preston tube to a point gage. Depth measurements were taken with a separate point gage. Figure 4.2 illustrates the components of the Preston tube configuration.

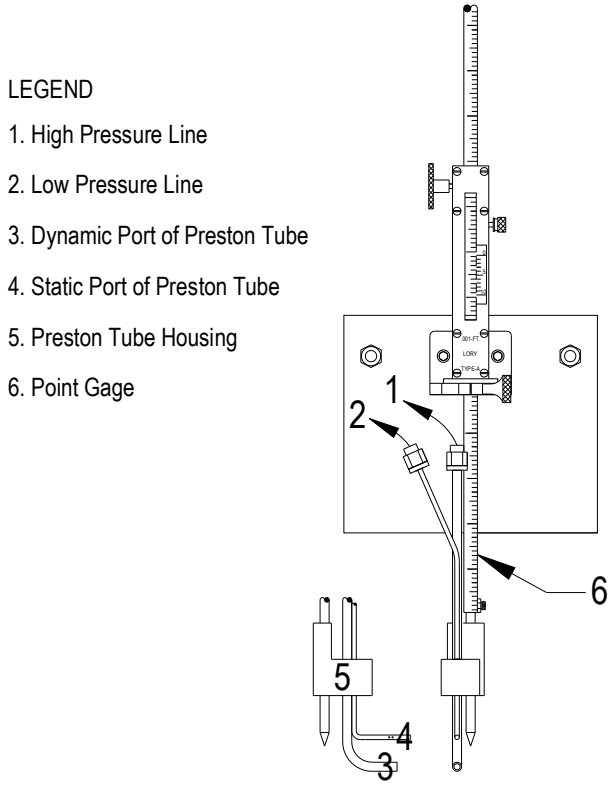

Figure 4.2: Preston tube configuration.

The outer diameter of the dynamic port of the Preston tube is 1/4 inch while the inside diameter of the dynamic port was 11/64 inch, creating an inside to outside diameter ratio of 0.69. Two static ports, each 1/32 inch in diameter, are located either

side of a 1/8 inch diameter tube, creating a total of four static ports for the Preston tube. A distance of 13/16 inch separate the static and dynamic ports. Figure 4.3 illustrates the dimensions of the Preston tube static and dynamic ports.

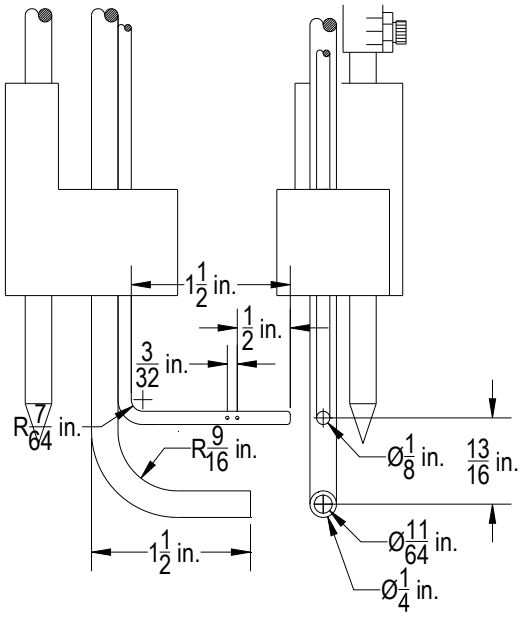

Figure 4.3: Dimensions of Preston tube.

4.4.2 DATA COLLECTION

Preston tube data were collected in the center of the flume, every two feet within the test section. Data was collected over a minute interval at a rate of 50 Hz; resulting in a raw data file with 3,000 data points at each station for a given discharge. An average of these 3,000 data points were taken and reported as voltage in a summary data file. Labview, a software created by National Instruments, Inc., was used to collect, organize, report, and partially process collected data.

High and low pressure lines from the Preston tube were connected to a 750 psi pressure transducer with an output range of 4 to 20 mA. Current from this transducer

was passed through a 250 ohm resistor which, from Ohm's law, converted the current to voltage. Therefore, a 4 to 20 mA signal was converted to 1 to 5 volts before the signal was sent to the computer. A data acquisition card was used to send the signal to Labview where the voltage was converted to differential pressure based on a given scale. For the 24-inch line, a maximum pressure differential was set to 3 inches. Conversion to differential pressure in inches took place within Labview based on Equation 4.1.

$$dH[in] = 0.75dV - 0.75 \qquad \textbf{Equation 4.1}$$

Where;

dH = differential head in inches; and

dV = differential voltage from input signal.

Note:

- The slope was computed as follows:

$$\frac{dP_{UPPERLIMIT} - dP_{LOWERLIMIT}}{dV_{UPPERLMIT} - dV_{LOWERLMIT}} = \frac{3in - 0in}{5V - 1V} = \frac{3in}{4V} = 0.75\,\tfrac{in}{V}$$

- The intercept was computed by knowing that at 5V there are 3in of differential pressure:

$$3in = 0.75(5V) + b$$
$$b = 3in - 0.75(5V) = -0.75$$

At lower discharges, the 6-inch line was used. Because the range of differential pressure was much lower for discharges run in the 6-inch line the upper limit was changed from 3

inches to 1.5 inches. Consequently, the conversion used in Labview was modified for the tests using the 6-inch line according to Equation 4.2.

$$dH[in] = 0.375dV - 0.375 \qquad \textbf{Equation 4.2}$$

Where;

dH = differential head in inches; and

dV = differential voltage from input signal.

Note:

- The slope was computed as follows:

$$\frac{dP_{UPPERLIMIT} - dP_{LOWERLIMIT}}{dV_{UPPERLMIT} - dV_{LOWERLMIT}} = \frac{1.5in - 0in}{5V - 1V} = \frac{1.5in}{4V} = 0.375\,\frac{in}{V}$$

- The intercept was computed by knowing that at 5V there are 3in of differential pressure:

$$1.5in = 0.375(5V) + b$$
$$b = 1.5in - 0.375(5V) = -0.375$$

Raw voltage and differential pressure, in inches, were reported in a summary file.

4.5 DISCHARGE MEASUREMENT

4.5.1 INTRODUCTION

Discharge data was recorded over a minute interval at a rate of 50 Hz resulting in 3,000 points. An average discharge reading was computed from the collected 3,000

points and reported to the summary file. Two separate discharge measurement devices were used; an Annubar for the 24-inch line, and an orifice plate for the 6-inch line. Both were placed approximately 21 feet downstream from the nearest disturbance.

4.5.2 ANNUBAR ON 24-INCH LINE

Discharge was measured in the 24-inch line using an Annubar, similar to what is depicted in Figure 4.4, designed and fabricated by Rosemount.

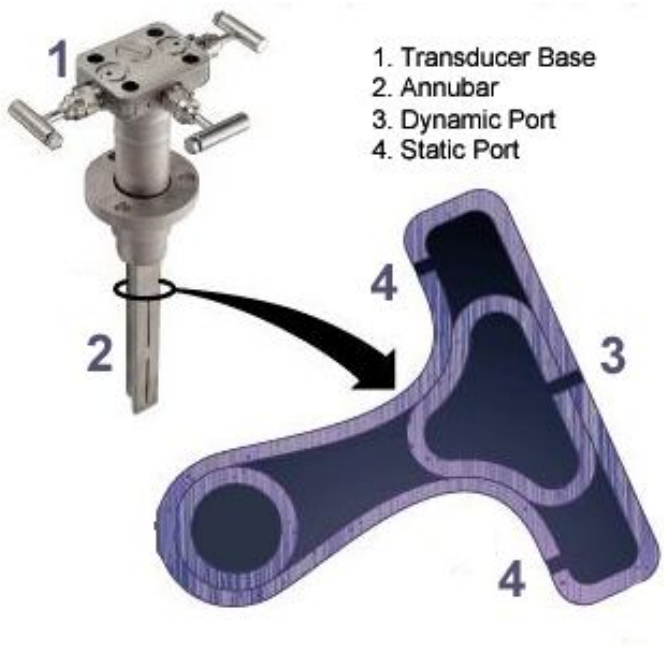

Figure 4.4: Diagram of Rosemount Annubar® configuration (Rosemount, 2002).

The annubar shown in Figure 4.4 works in a similar manner as the Preston tube. Dynamic ports located along the front of the Annubar read the total pressure and two static ports located on the back of the Annubar read the static pressure. Differential pressure is then determined using a pressure transducer, which outputs 0 mA to 20 mA current. A 3,626 psi pressure transducer, used for differential pressure measurement,

produced a square root transformed signal before being sent to the readout box. Current from the transducer was passed through a 250 ohm resister to convert it to voltage before ultimately being sent to the data acquisition card on the computer. A discharge range from from 0 cfs to 24.5 cfs set for the transducer dictated the conversion shown in Equation 4.3 from voltage to discharge.

$$Q[cfs] = 6.125dV - 6.125 \qquad \textbf{Equation 4.3}$$

Where;

$Q =$ discharge in cfs; and

$dV =$ differential voltage from input signal.

Note:

- The slope was computed as follows:

$$\frac{Q_{UPPERLIMIT} - Q_{LOWERLIMIT}}{dV_{UPPERLMIT} - dV_{LOWERLMIT}} = \frac{24.5cfs - 0cfs}{5V - 1V} = \frac{24.4cfs}{4V} = 6.125\frac{cfs}{V}$$

- The intercept was computed by knowing that at 5V there are 3in of differential pressure:

$$24.5cfs = 6.125(5V) + b$$
$$b = 24.5cfs - 6.125(5V) = -6.125$$

4.5.3 ORIFICE PLATE ON THE 6-INCH LINE

Discharge was measured in the 6-inch line using a 6-inch by 4.33-inch orifice plate, which measures differential pressure across an abrupt constriction in flow. A 3,626 psi transducer was used to convert the differential pressure to a 0 mA to 20 mA signal. The maximum discharge set for the orifice plate was 4.774 cfs. A square root signal was sent from the transducer, through a 250 ohm resister to convert it to voltage, and then to the data acquisition card in the computer. Within Labview, the input voltage was converted to discharge using Equation 4.4.

$$Q[cfs] = 1.1935dV - 1.1935 \qquad \textbf{Equation 4.4}$$

Where;

$Q =$ discharge in cfs; and

$dV =$ differential voltage from input signal.

Note:

- The slope was computed as follows:

$$\frac{Q_{UPPERLIMIT} - Q_{LOWERLIMIT}}{dV_{UPPERLMIT} - dV_{LOWERLMIT}} = \frac{4.774cfs - 0cfs}{5V - 1V} = \frac{4.774cfs}{4V} = 1.1935\frac{cfs}{V}$$

- The intercept was computed by knowing that at 5V there are 3in of differential pressure:

$$4.774cfs = 1.1935(5V) + b$$
$$b = 4.774cfs - 1.1935(5V) = -1.1935$$

5 TEST MATRIX

Calibration of the Preston tube required that a certain range of pressure readings be correlated with shear stress readings. For this research, calibration of the Preston tube is tailored specifically to support work being performed at CSU on the Middle Rio Grande model. Two distinct bed characteristics were created for calibrating the Preston tube, a gravel bed and a concrete cap. The gravel bed, corresponding to the native topography research on the Rio Grande model, is expected to have Preston tube measurements ranging from 0 in to 1.5 in. The concrete cap corresponds to previous work on the Middle Rio Grande, where the channel cross section was trapezoidal in shape and the surface was brushed concrete. Preston tube readings for concrete surface ranged from 0 in to 0.44 in. With the slope of the bed held constant, discharge and backwater was altered to achieve the desired Preston tube ranges.

A range of discharges were modeled in the 4-foot flume, including 2 cfs, 5 cfs, 7 cfs, 9 cfs, 12 cfs, and 15 cfs. For the gravel bed, 20 cfs and 22 cfs were also included to achieve higher Preston tube readings. Additional tests were conducted with the backwater approximately set, using the downstream sluice gate, to normal depth. Three tests were run for the gravel bed using normal depth backwater conditions: 5cfs with 0.9 ft backwater, 9cfs with 1.3 ft backwater and 15 cfs with 1.5 ft backwater. Three tests were also run for the concrete cap with normal depth backwater conditions: 5cfs with

1.05 ft backwater, 9cfs with 1.28 ft backwater, and 12 cfs with 1.73 ft backwater. Figure 5.1 summarizes the test matrix for the Preston tube calibration in the 4-foot flume.

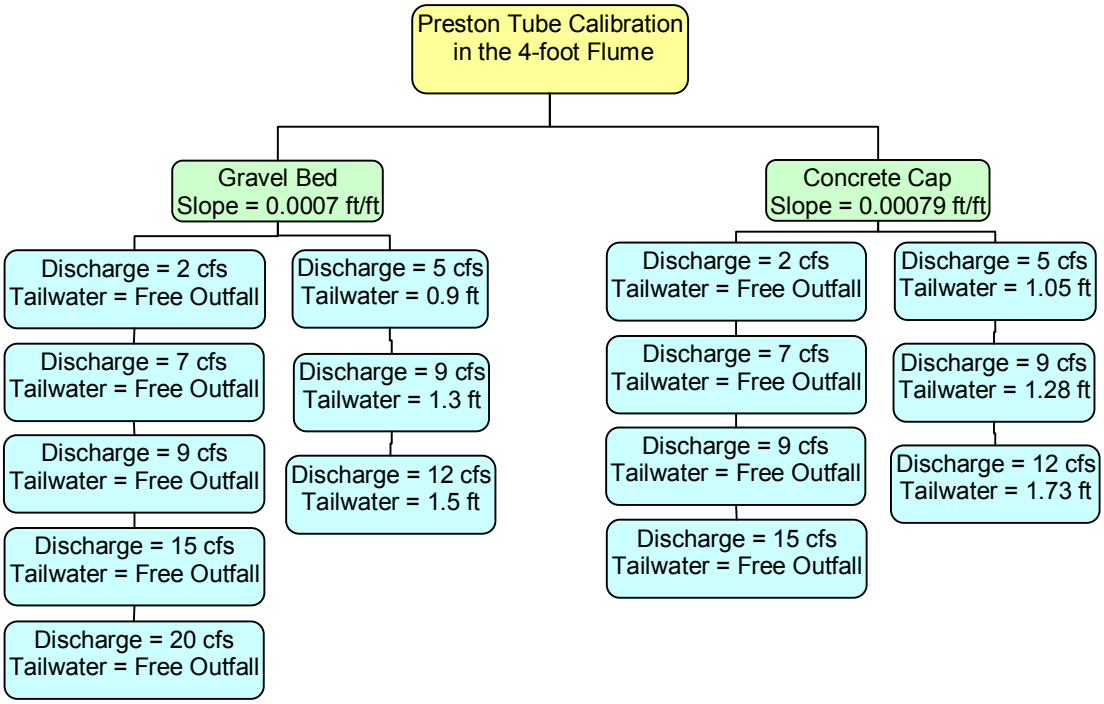

Figure 5.1: Test matrix for the Preston tube calibration in the 4-foot flume.

6 RESULTS

6.1 INTRODUCTION

Procedures outlined for collecting water surface profiles, boundary shear stress computations, and Preston tube measurements in Section 4 were used for the gravel bed and the concrete cap for each test in Figure 5.1. Development of a final calibration curve used the Preston tube data, averaged over 60 second intervals, with the computed shear stress values from the normalized water surface profiles. Water surface profiles; both measured and computed, shear stress computations, and Preston tube data are presented in this section. Section 7 integrates shear stress computations with Preston tube data, creating the calibration curve.

6.2 MANNING'S ROUGHNESS

Using standard step backwater computations (Chow, 1959), a computed water surface profile was developed for each test to match the measured water surface profile. Error, defined as the sum of the square differences between computed and measured water surface profiles, was determined for each backwater computation. Manning's roughness was adjusted until the error was reduced to a minimum. As a result, each test included a distinct Manning's Roughness value. For the gravel bed, Manning's roughness values are summarized in Table 6.1 and for the concrete cap, Manning's roughness values are summarized in Table 6.2.

Table 6.1: Manning's roughness for the gravel bed.

Discharge, Q (cfs)	Backwater Conditions	Manning's Roughness
2	Free Outfall	0.021
5	Free Outfall	0.024
7	Free Outfall	0.026
9	Free Outfall	0.024
12	Free Outfall	0.025
15	Free Outfall	0.025
20	Free Outfall	0.025
22	Free Outfall	0.024
5	0.9 ft	0.027
9	1.3 ft	0.030
12	1.5 ft	0.030

Table 6.2: Manning's roughness values for the concrete cap.

Discharge, Q (cfs)	Backwater Conditions	Manning's Roughness
2	Free Outfall	0.017
5	Free Outfall	0.021
7	Free Outfall	0.022
9	Free Outfall	0.022
12	Free Outfall	0.022
15	Free Outfall	0.022
5	1.05 ft	0.032
9	1.28 ft	0.026
15	1.73 ft	0.024

6.3 DEPTH

Water surface profiles were computed using Manning's roughness values summarized in Table 6.1 and Table 6.2. Downstream boundary conditions for tests with no backwater were taken from measured depth information at the downstream station.

Downstream boundary conditions for tests with backwater set to normal depth were taken from measured depth, averaged over the test section. Figure 6.1 shows a plot of the measured and normalized gravel bed depths plotted together for each test with no backwater conditions.

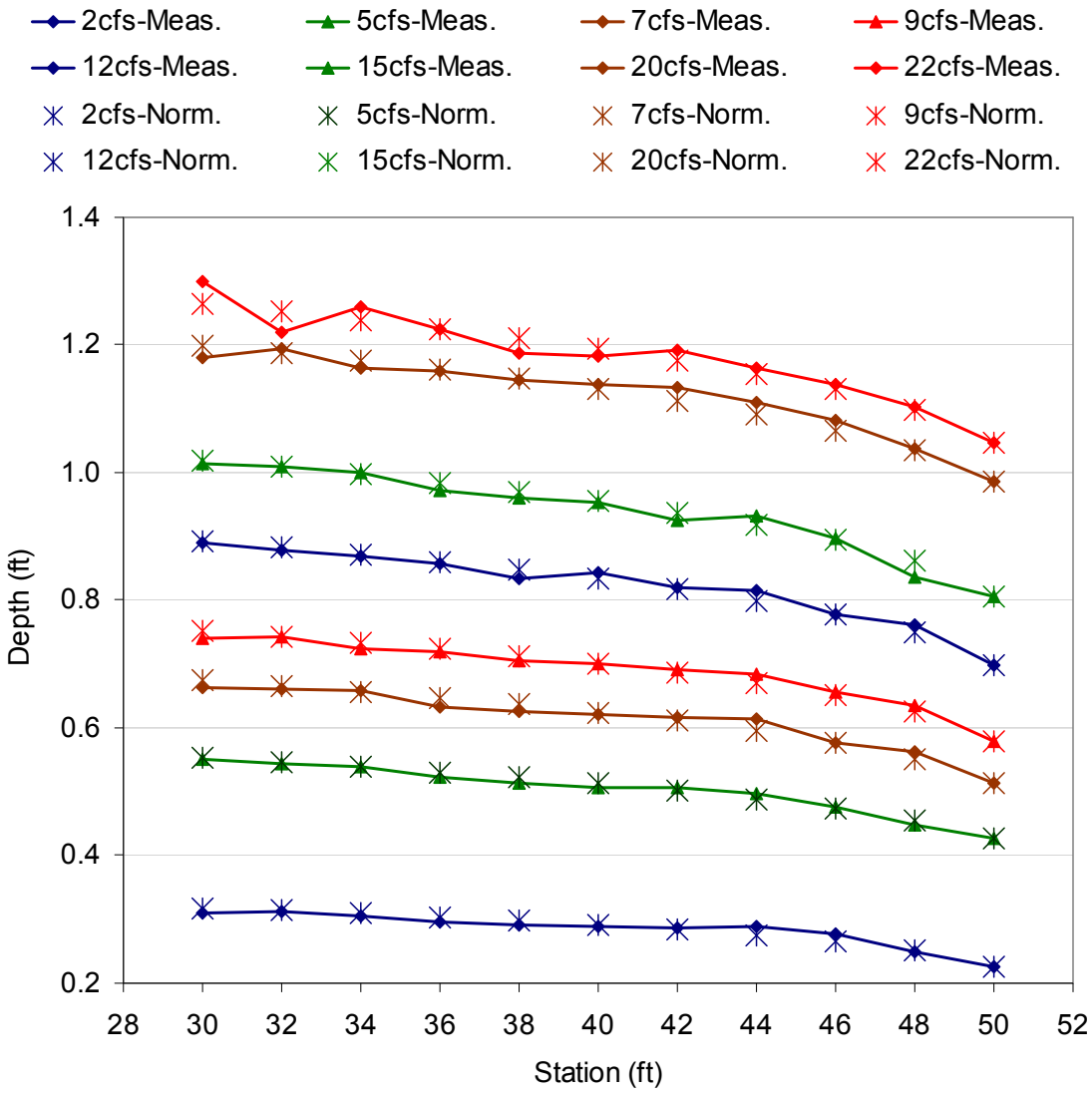

Figure 6.1: Gravel bed measured and normalized depths for free outfall conditions.

Measured and normalized depths for tests with backwater set to normal depth for the gravel bed are plotted in Figure 6.2.

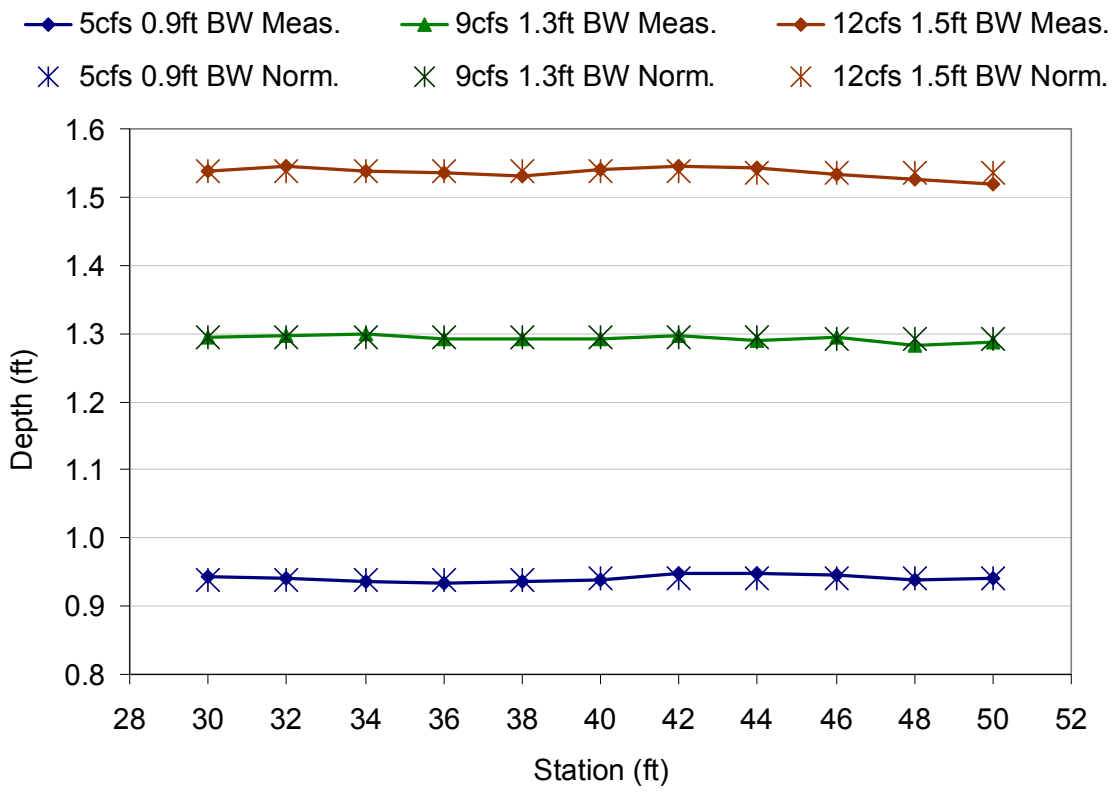

Figure 6.2: Gravel bed measured and normalized depths for normal depth backwater conditions.

Percent differences between the measured depth and the normalized depth were computed for each discharge at each station. Percent differences for gravel bed depths with no backwater are presented in Table 6.3.

Table 6.3: Percent differences for gravel bed depths with free outfall conditions.

Station (ft)	2cfs	5cfs	7cfs	9cfs	12cfs	15cfs	20cfs	22cfs
30	2.55%	0.18%	1.58%	1.53%	0.22%	0.41%	1.61%	2.74%
32	0.51%	0.21%	0.92%	0.23%	0.46%	0.06%	0.65%	2.51%
34	0.96%	0.04%	0.31%	1.29%	0.50%	0.23%	0.92%	1.58%
36	2.64%	1.49%	2.23%	0.72%	0.44%	1.25%	0.28%	0.05%
38	2.10%	1.57%	1.82%	1.15%	1.82%	0.98%	0.22%	2.01%
40	0.95%	1.05%	0.55%	0.03%	1.05%	0.12%	0.76%	1.07%

42	0.55%	1.11%	0.83%	0.75%	0.09%	1.30%	1.84%	1.22%
44	4.56%	1.66%	3.06%	1.96%	1.97%	1.60%	1.68%	0.64%
46	4.61%	0.28%	0.06%	0.77%	0.10%	0.22%	1.52%	0.57%
48	0.36%	1.44%	1.80%	1.42%	1.76%	3.02%	0.32%	0.44%
50	0.00%	0.00%	0.00%	0.00%	0.00%	0.00%	0.00%	0.00%
Average:	**1.80%**	**0.82%**	**1.20%**	**0.90%**	**0.76%**	**0.84%**	**0.89%**	**1.17%**

Table 6.4 presents percent differences for gravel bed depths with normal depth backwater conditions.

Table 6.4: Percent differences for gravel bed depths with normal depth backwater conditions.

Station (ft)	5cfs-0.9ft	9cfs-1.3ft	12cfs-1.5ft
30	0.43%	0.10%	0.06%
32	0.10%	0.16%	0.48%
34	0.45%	0.25%	0.08%
36	0.58%	0.19%	0.13%
38	0.49%	0.24%	0.50%
40	0.08%	0.07%	0.17%
42	0.86%	0.26%	0.58%
44	0.73%	0.26%	0.34%
46	0.61%	0.08%	0.22%
48	0.15%	0.76%	0.72%
50	0.06%	0.35%	1.03%
Average:	**0.41%**	**0.25%**	**0.39%**

Concrete cap measured and normalized depths for free outfall conditions are plotted in Figure 6.3.

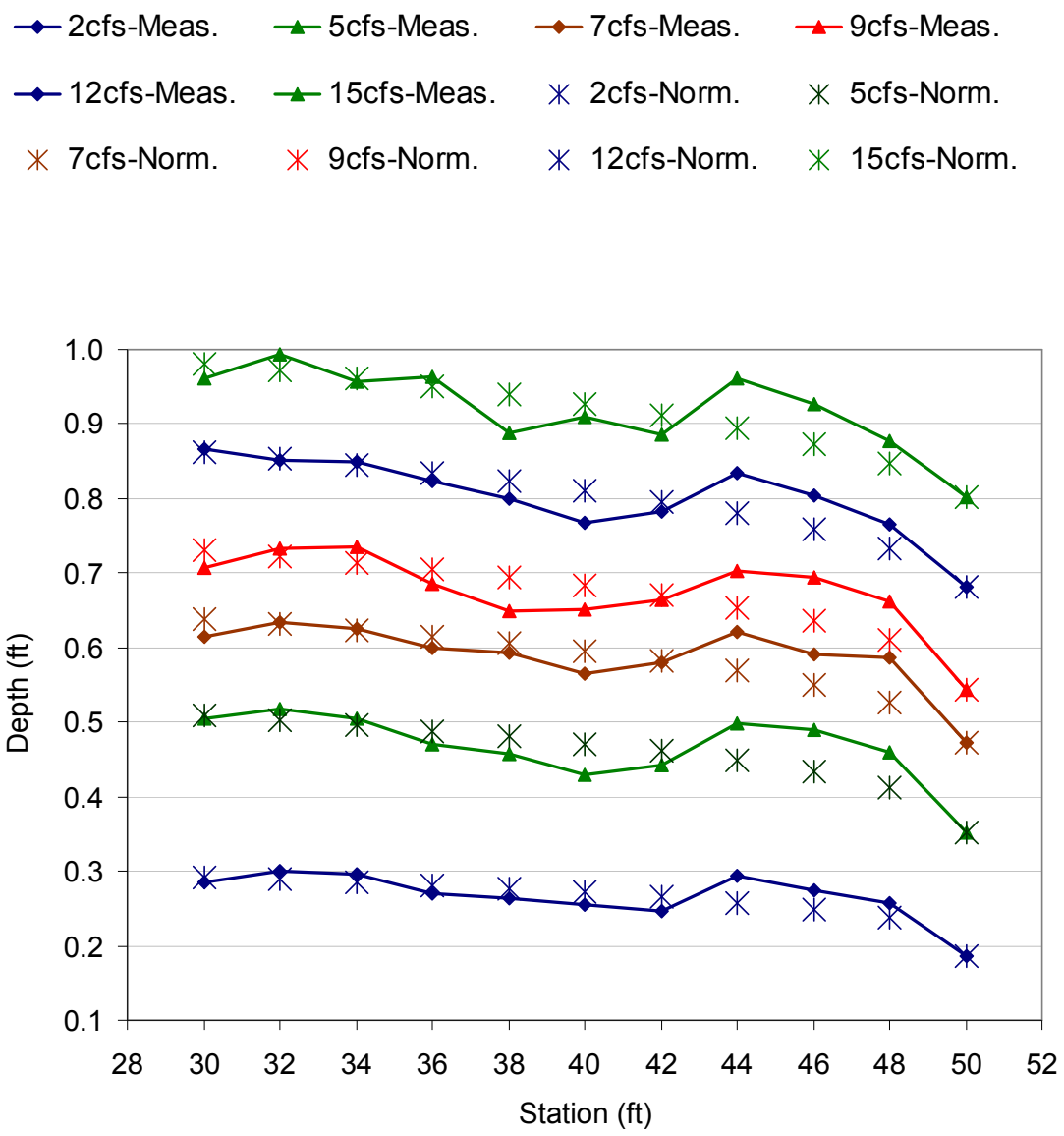

Figure 6.3: Concrete cap measured and normalized depths for free outfall conditions.

Concrete cap measured and normalized depths from tests with backwater conditions set to normal depth are plotted in Figure 6.4.

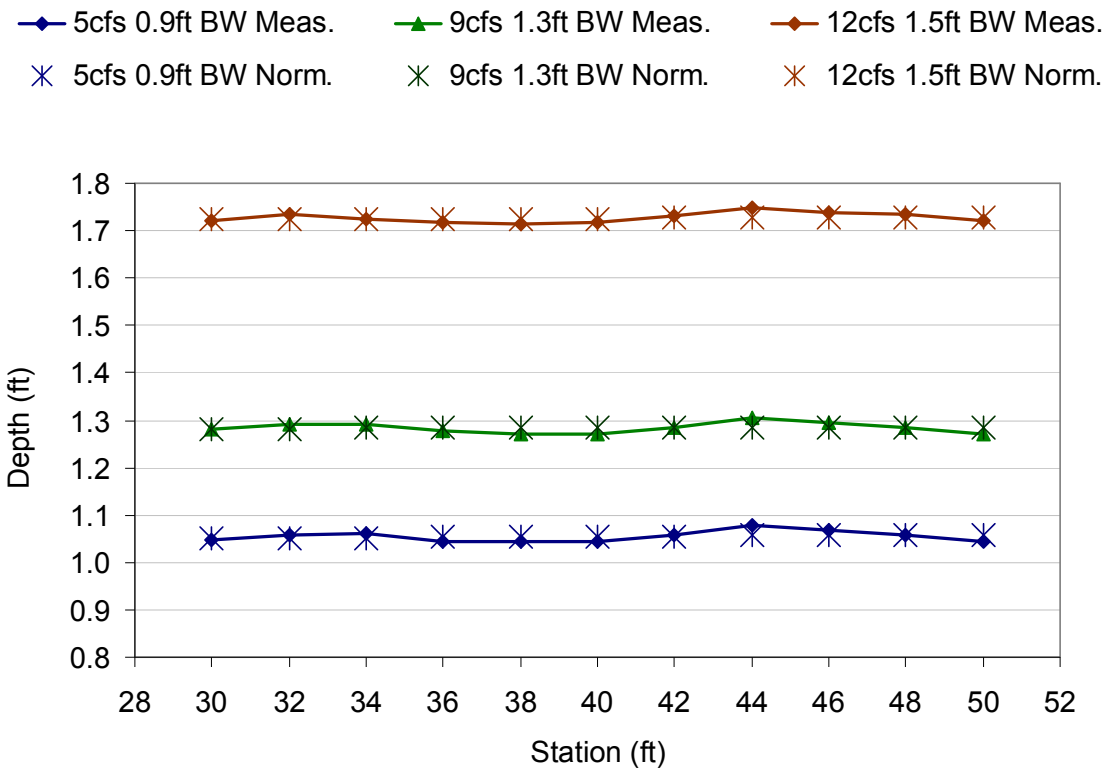

Figure 6.4: Concrete cap measured and normalized depths for normal depth backwater conditions.

Percent differences between the measured and normalized depths on the concrete cap with no backwater are summarized in Table 6.5.

Table 6.5: Percent differences for concrete cap depths with free outfall conditions.

Station (ft)	2cfs	5cfs	7cfs	9cfs	12cfs	15cfs
30	2.33%	0.65%	4.06%	3.25%	0.38%	2.14%
32	3.61%	3.05%	0.23%	1.51%	0.34%	2.20%
34	3.25%	1.87%	0.38%	2.95%	0.54%	0.64%
36	4.17%	3.90%	2.49%	2.75%	1.36%	1.22%
38	4.78%	4.87%	2.27%	6.84%	2.86%	5.91%
40	6.44%	9.61%	5.08%	4.90%	5.52%	1.90%

42	7.44%	4.31%	0.45%	0.72%	1.69%	2.87%
44	11.86%	9.85%	8.62%	6.79%	6.62%	7.03%
46	9.32%	11.26%	6.64%	8.45%	5.40%	5.64%
48	7.72%	10.18%	10.26%	7.81%	4.22%	3.54%
50	0.00%	0.00%	0.00%	0.00%	0.00%	0.00%
Average:	**5.54%**	**5.41%**	**3.68%**	**4.18%**	**2.63%**	**3.01%**

Concrete cap percent differences between measured and normalized depths with normal depth backwater conditions are summarized in Table 6.6.

Table 6.6: Percent differences for concrete cap depths with normal depth backwater conditions.

Station (ft)	5cfs-0.9ft	9cfs-1.3ft	12cfs-1.5ft
30	0.37%	0.11%	0.22%
32	0.68%	0.71%	0.51%
34	0.78%	0.53%	0.09%
36	0.83%	0.51%	0.35%
38	1.01%	0.93%	0.66%
40	1.10%	1.12%	0.45%
42	0.25%	0.12%	0.34%
44	1.93%	1.54%	1.34%
46	1.11%	0.75%	0.69%
48	0.01%	0.03%	0.44%
50	1.44%	1.10%	0.33%
Average:	**0.86%**	**0.68%**	**0.49%**

6.3.1 SHEAR STRESS

From normalized water surface profiles, boundary shear stress was computed by using the momentum equation presented in Equation 2.12 for rectangular channels with

plexiglass left and right walls. Computation of the boundary shear stress utilized 0.2 ft control volumes for the entire test reach. Boundary shear stress at each data location station shown in Figure 4.1 was determined by averaging computed boundary shear stress values from the control volume upstream and downstream of the data. Computed gravel bed boundary shear stress values for tests with no backwater conditions are presented in Table 6.7.

Table 6.7: Gravel bed boundary shear stress values for no backwater conditions.

Station (ft)	2cfs	5cfs	7cfs	9cfs	12cfs	15cfs	20cfs	22cfs
30	0.045	0.104	0.147	0.157	0.203	0.238	0.287	0.290
32	0.047	0.107	0.152	0.162	0.209	0.244	0.293	0.296
34	0.048	0.111	0.157	0.167	0.214	0.251	0.300	0.303
36	0.050	0.115	0.162	0.173	0.221	0.259	0.308	0.311
38	0.052	0.120	0.169	0.179	0.229	0.268	0.317	0.319
40	0.055	0.125	0.177	0.186	0.239	0.278	0.328	0.329
42	0.059	0.132	0.186	0.195	0.249	0.290	0.340	0.341
44	0.063	0.140	0.197	0.207	0.263	0.305	0.356	0.356
46	0.069	0.150	0.213	0.221	0.281	0.324	0.376	0.375
48	0.079	0.166	0.236	0.244	0.307	0.353	0.403	0.401
50	0.100	0.192	0.279	0.289	0.359	0.411	0.452	0.449
Average:	**0.052**	**0.119**	**0.168**	**0.178**	**0.228**	**0.267**	**0.316**	**0.318**

Note: Shear stress for stations 46-50 were excluded from averages to eliminate effects of downstream transition.

Table 6.8 presents the computed gravel bed boundary shear stress values for backwater conditions set to normal depth.

Table 6.8: Gravel bed boundary shear stress values for normal depth backwater conditions.

Station (ft)	5cfs 0.9ft BW	9cfs 1.3ft BW	12cfs 1.5ft BW

30	0.038	0.068	0.083
32	0.038	0.068	0.083
34	0.038	0.068	0.083
36	0.038	0.068	0.083
38	0.038	0.068	0.083
40	0.038	0.068	0.083
42	0.038	0.068	0.083
44	0.038	0.069	0.083
46	0.038	0.069	0.083
48	0.038	0.069	0.083
50	0.037	0.069	0.084
Average:	**0.038**	**0.068**	**0.083**

Note: Shear stress for stations 46-50 were excluded from averages to eliminate effects of downstream transition.

Data presented in Table 6.7 and Table 6.8 are shown, graphically, in Figure 6.5 and Figure 6.6, respectively.

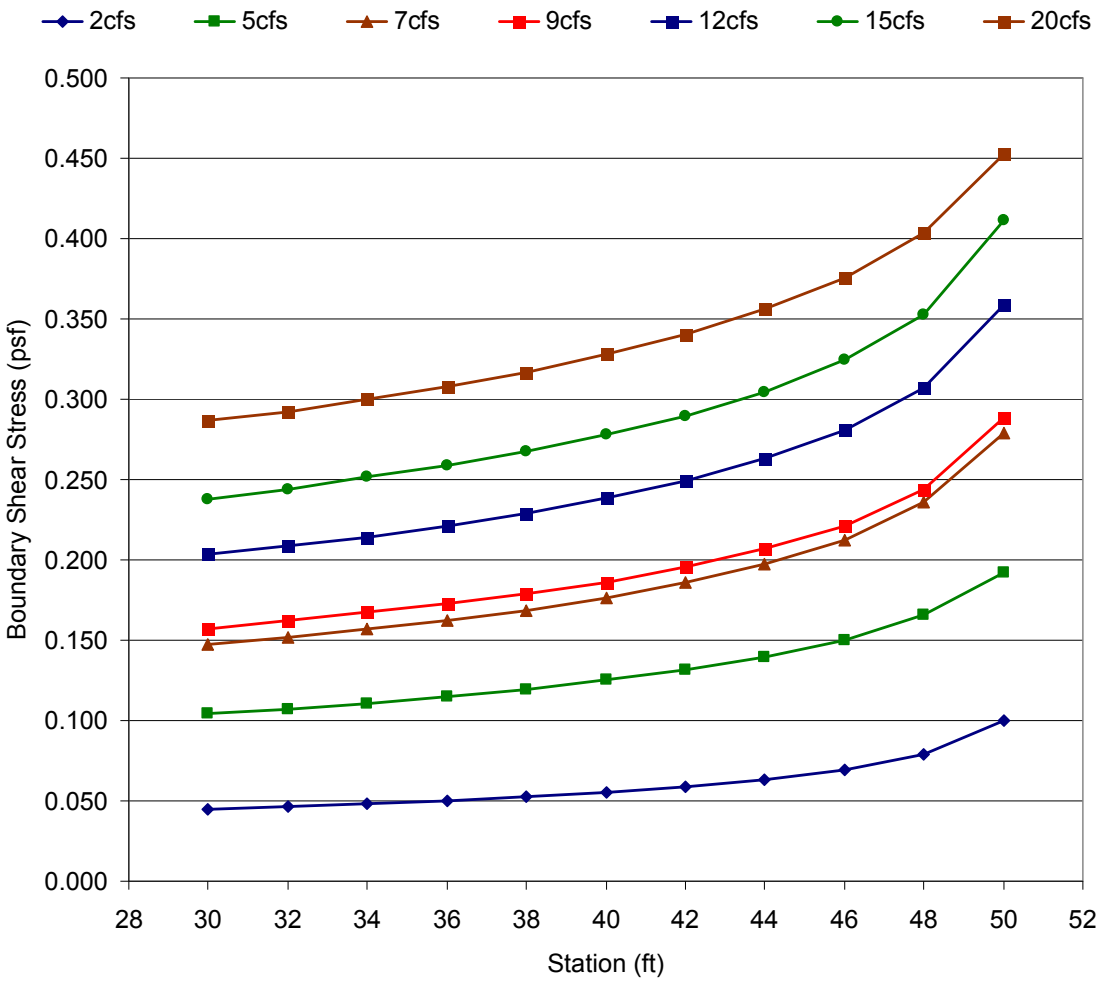

Figure 6.5: Gravel bed computed boundary shear stress for no backwater conditions.

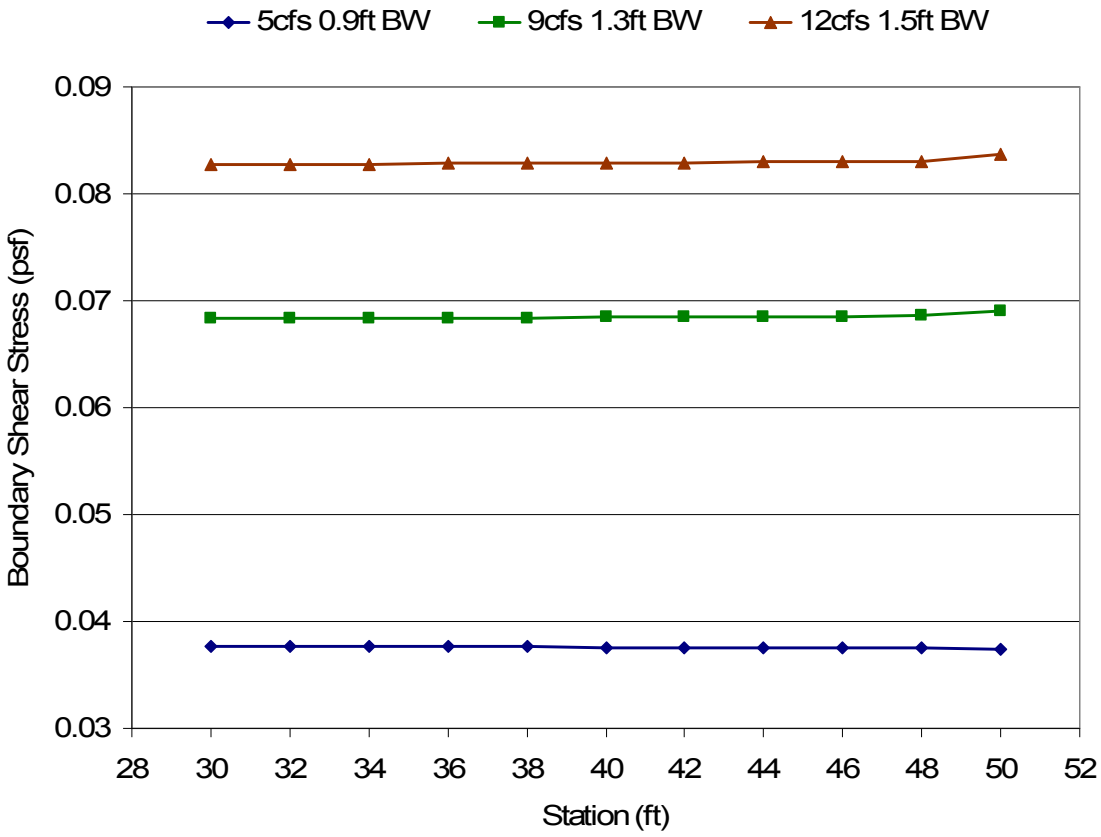

Figure 6.6: Gravel bed boundary shear stress for normal depth backwater conditions.

Concrete cap bound\ary shear stress values with no backwater conditions are presented in Table 6.9.

Table 6.9: Concrete cap boundary shear stress values for no backwater conditions.

Station (ft)	2cfs	5cfs	7cfs	9cfs	12cfs	15cfs
30	0.035	0.087	0.120	0.142	0.171	0.197
32	0.036	0.089	0.124	0.145	0.175	0.202
34	0.037	0.092	0.127	0.149	0.180	0.207
36	0.039	0.095	0.131	0.154	0.185	0.212
38	0.040	0.099	0.136	0.160	0.191	0.219
40	0.042	0.103	0.142	0.166	0.198	0.226

42	0.045	0.109	0.149	0.174	0.206	0.235
44	0.047	0.115	0.158	0.183	0.217	0.246
46	0.052	0.125	0.170	0.197	0.231	0.259
48	0.058	0.140	0.189	0.217	0.251	0.279
50	0.101	0.198	0.240	0.277	0.296	0.317
Average:	**0.040**	**0.098**	**0.136**	**0.159**	**0.191**	**0.218**

Note: Shear stress for stations 46-50 were excluded from averages to eliminate effects of downstream transition.

Table 6.10 presents concrete cap boundary shear stress values with backwater conditions set to normal depth.

Table 6.10: Concrete cap boundary shear stress values for normal depth backwater conditions.

Station (ft)	5cfs-1.05ft	9cfs-1.28ft	15cfs-1.73ft
30	0.023	0.050	0.065
32	0.023	0.050	0.065
34	0.023	0.050	0.065
36	0.023	0.050	0.065
38	0.023	0.050	0.065
40	0.023	0.050	0.065
42	0.023	0.050	0.065
44	0.023	0.050	0.065
46	0.023	0.050	0.065
48	0.023	0.050	0.065
50	0.022	0.049	0.064
Average:	**0.023**	**0.050**	**0.065**

Note: Shear stress for stations 46-50 were excluded from averages to eliminate effects of downstream transition.

Table 6.9 and Table 6.10 are presented graphically in Figure 6.7 and Figure 6.8, respectively.

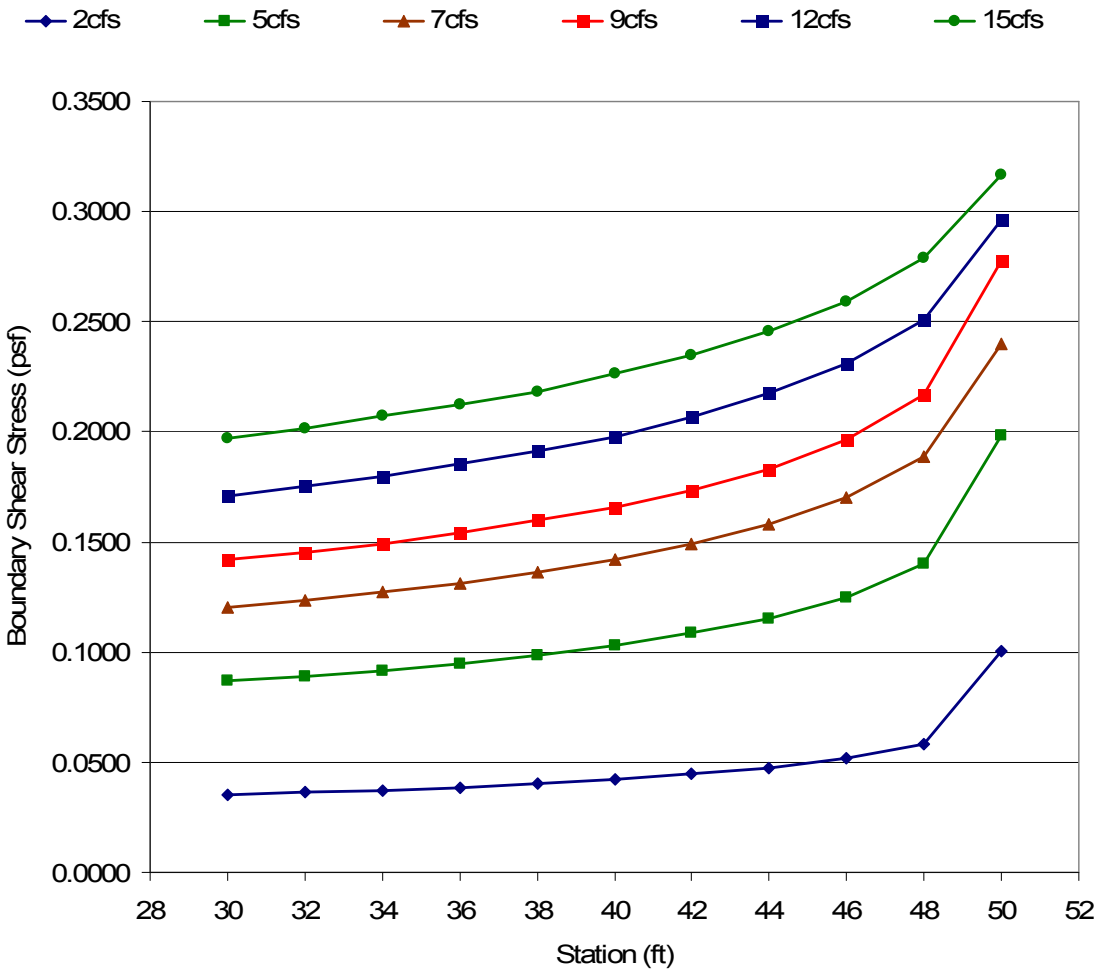

Figure 6.7: Concrete cap boundary shear stress with no backwater conditions.

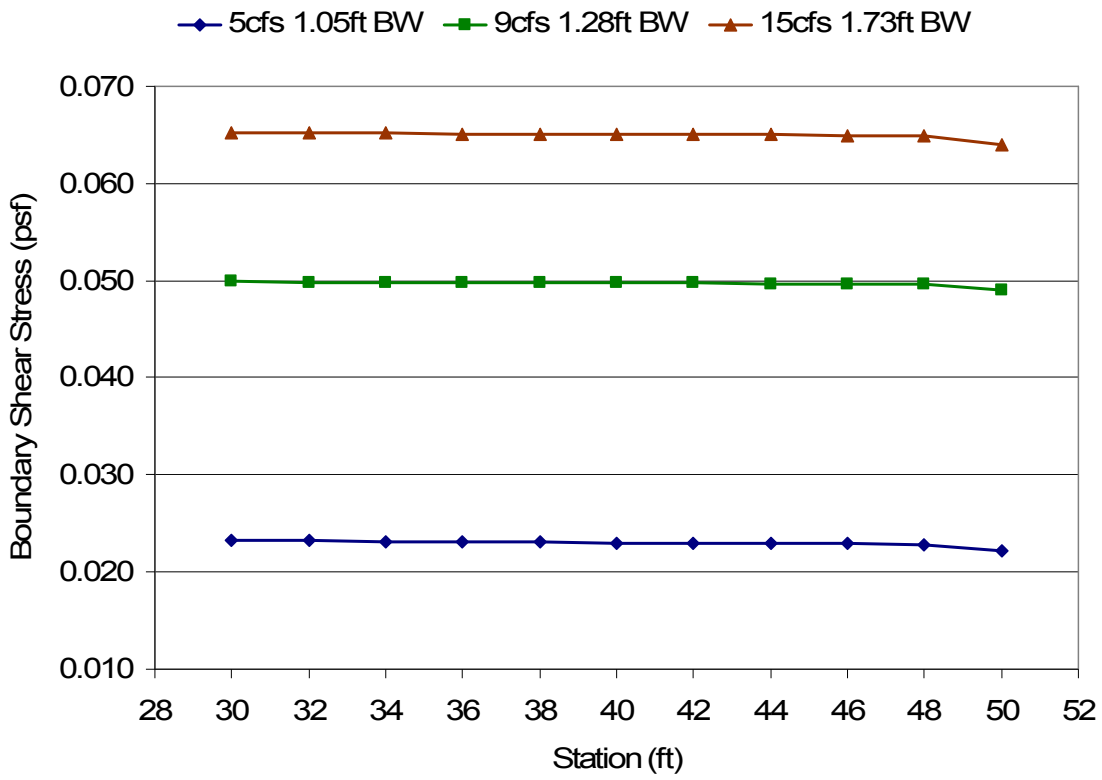

Figure 6.8: Concrete cap boundary shear stress with backwater set to normal depth.

6.3.2 PRESTON TUBE DATA

Differential pressure between the high and low pressure port on the Preston tube was recorded in the center of the 4-foot flume for each data point in Figure 4.1. Differential pressure readings were taken in one minute intervals at a rate of 50 Hz; resulting in 3000 readings. An average of the 3000 differential pressure readings taken from the Preston tube was recorded in a summary file and used for the final calibration curve. Differential pressure readings were recorded in inches of pressure head. For each test in Figure 5.1, eleven (11) average differential pressure readings were recorded for the data locations within the test section. Average Preston tube measurements for the gravel bed with no backwater are presented in Table 6.11.

Table 6.11: Gravel bed Preston tube measurements for no backwater conditions.

Station (ft)	2cfs	5cfs	7cfs	9cfs	12cfs	15cfs	20cfs	22cfs
30	0.170	0.387	0.503	0.575	0.695	0.906	0.995	0.889
32	0.151	0.325	0.483	0.460	0.681	0.969	1.002	1.048
34	0.205	0.410	0.487	0.548	0.668	0.838	0.990	0.915
36	0.196	0.403	0.562	0.666	0.809	0.983	1.029	1.024
38	0.238	0.412	0.520	0.681	0.775	0.842	1.175	1.138
40	0.253	0.497	0.665	0.660	0.757	0.873	1.286	1.122
42	0.233	0.437	0.546	0.582	0.811	0.933	1.064	0.951
44	0.226	0.401	0.599	0.659	0.702	1.053	1.167	1.082
46	0.324	0.577	0.728	0.849	0.990	1.069	1.290	1.270
48	0.389	0.768	0.724	0.798	1.026	1.375	1.214	1.400
50	0.437	0.790	1.041	1.193	1.305	1.566	1.947	1.731
Average:	**0.209**	**0.409**	**0.546**	**0.604**	**0.737**	**0.925**	**1.089**	**1.021**

Note: Shear stress for stations 46-50 were excluded from averages to eliminate effects of downstream transition.

Table 6.12 presents average Preston tube measurements for the gravel bed with backwater set to normal depth.

Table 6.12: Gravel bed Preston tube measurements for normal depth backwater conditions.

Station (ft)	5cfs 0.9ft BW	9cfs 1.3ft BW	12cfs 1.5ft BW
30	0.110	0.205	0.256
32	0.101	0.154	0.230
34	0.101	0.212	0.261
36	0.118	0.195	0.255
38	0.103	0.196	0.262
40	0.114	0.207	0.295
42	0.114	0.158	0.248
44	0.097	0.156	0.200

46	0.109	0.189	0.270
48	0.141	0.193	0.282
50	0.117	0.191	0.244
Average:	**0.107**	**0.185**	**0.251**

Note: Shear stress for stations 46-50 were excluded from averages to eliminate effects of downstream transition.

Table 6.11 and Table 6.12 are presented graphically in Figure 6.9 and Figure 6.10, resptively.

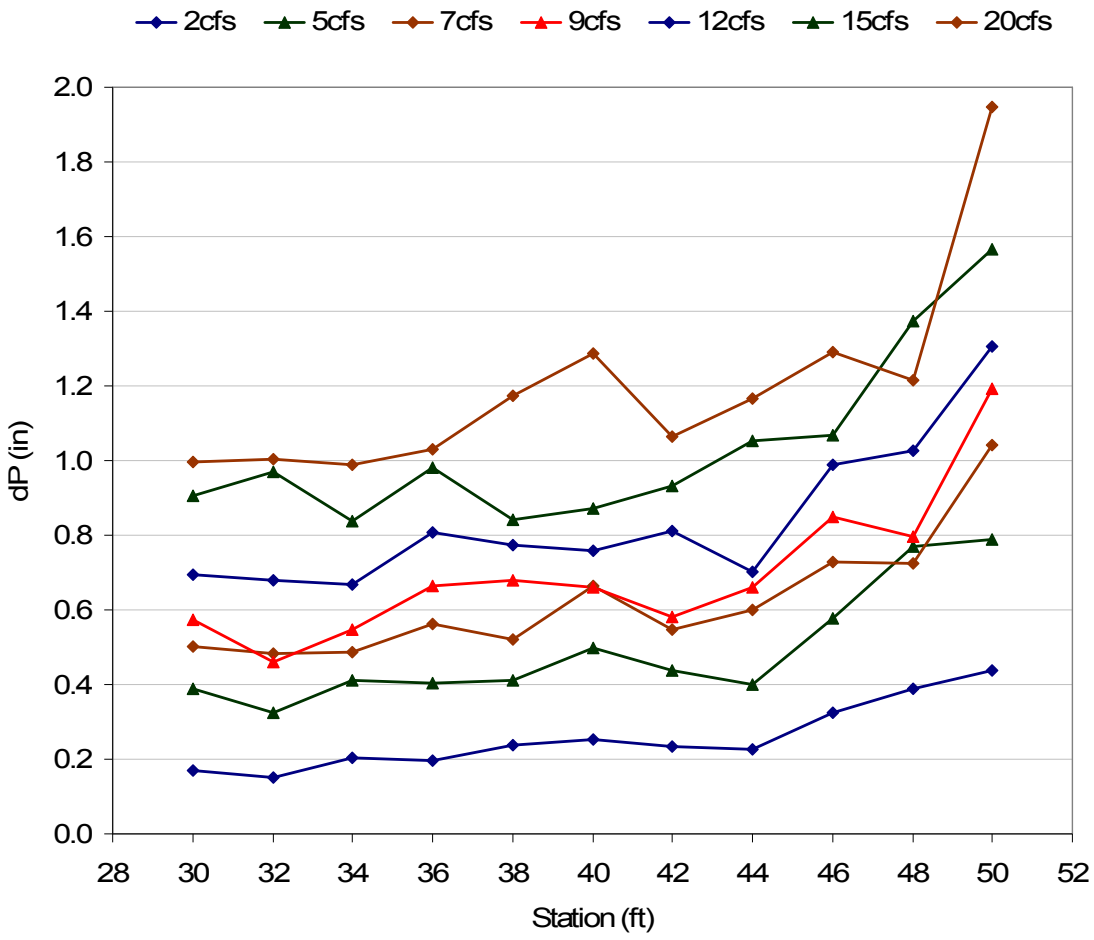

Figure 6.9: Gravel bed Preston tube measurements with no backwater conditions.

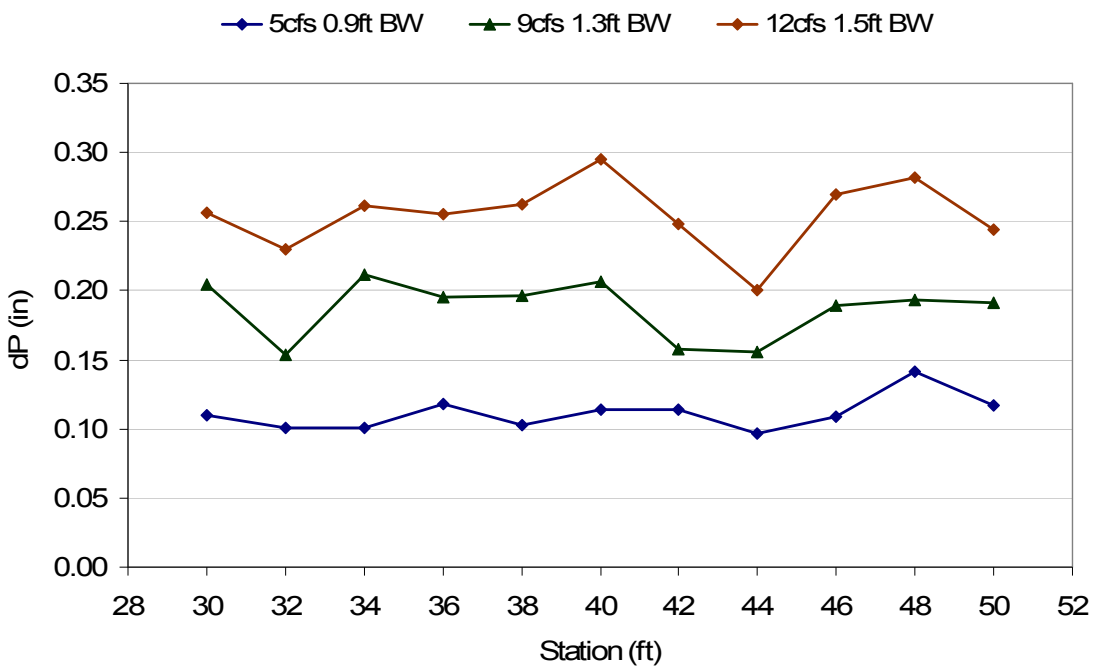

Figure 6.10: Gravel bed Preston tube measurements with normal depth backwater conditions.

Concrete cap averaged Preston tube measurements with no backwater conditions are presented in Table 6.13.

Table 6.13: Concrete cap Preston tube measurements with no backwater conditions.

Station (ft)	2cfs	5cfs	7cfs	9cfs	12cfs	15cfs
30	0.236	0.585	0.941	1.164	1.238	1.394
32	0.206	0.513	0.768	0.876	0.950	1.271
34	0.349	0.532	0.796	0.904	1.037	1.332
36	0.335	0.712	0.923	1.070	1.210	1.326
38	0.244	0.599	0.807	1.117	1.127	1.441
40	0.283	0.729	0.917	0.935	1.136	1.290
42	0.238	0.638	0.771	0.906	1.025	1.396
44	0.194	0.444	0.654	0.783	0.908	1.072
46	0.327	0.517	0.844	0.994	1.141	1.468

48	0.379	0.607	0.841	1.054	1.259	1.547
50	0.688	1.617	1.871	2.012	1.947	2.222
Average:	**0.261**	**0.594**	**0.822**	**0.969**	**1.079**	**1.315**

Note: Shear stress for stations 46-50 were excluded from averages to eliminate effects of downstream transition.

Table 6.14 presents Concrete cap averaged Preston tube measurements for backwater conditions set to normal depth.

Table 6.14: Concrete cap Preston tube measurements with normal depth backwater conditions.

Station (ft)	5cfs 1.05ft BW	9cfs 1.28ft BW	15cfs 1.73ft BW
30	0.185	0.379	0.549
32	0.167	0.360	0.503
34	0.148	0.324	0.484
36	0.188	0.384	0.500
38	0.143	0.299	0.449
40	0.148	0.322	0.392
42	0.141	0.270	0.426
44	0.134	0.292	0.402
46	0.158	0.337	0.434
48	0.164	0.316	0.413
50	0.165	0.379	0.518
Average:	**0.157**	**0.329**	**0.463**

Note: Shear stress for stations 46-50 were excluded from averages to eliminate effects of downstream transition.

Table 6.13 and Table 6.14 are presented graphically in Figure 6.11 and Figure 6.12, respectively.

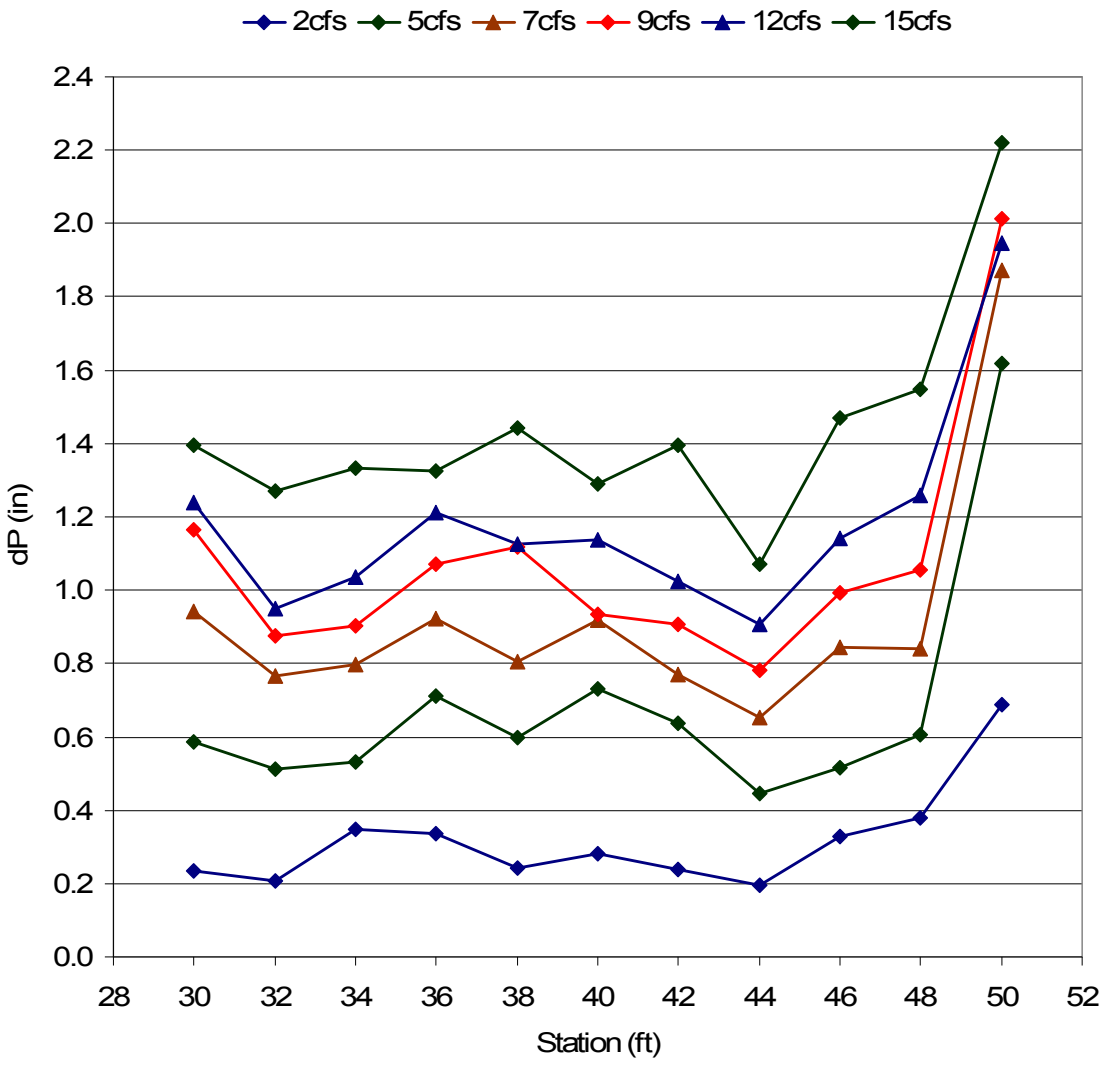

Figure 6.11: Concrete cap Preston tube measurements with no backwater.

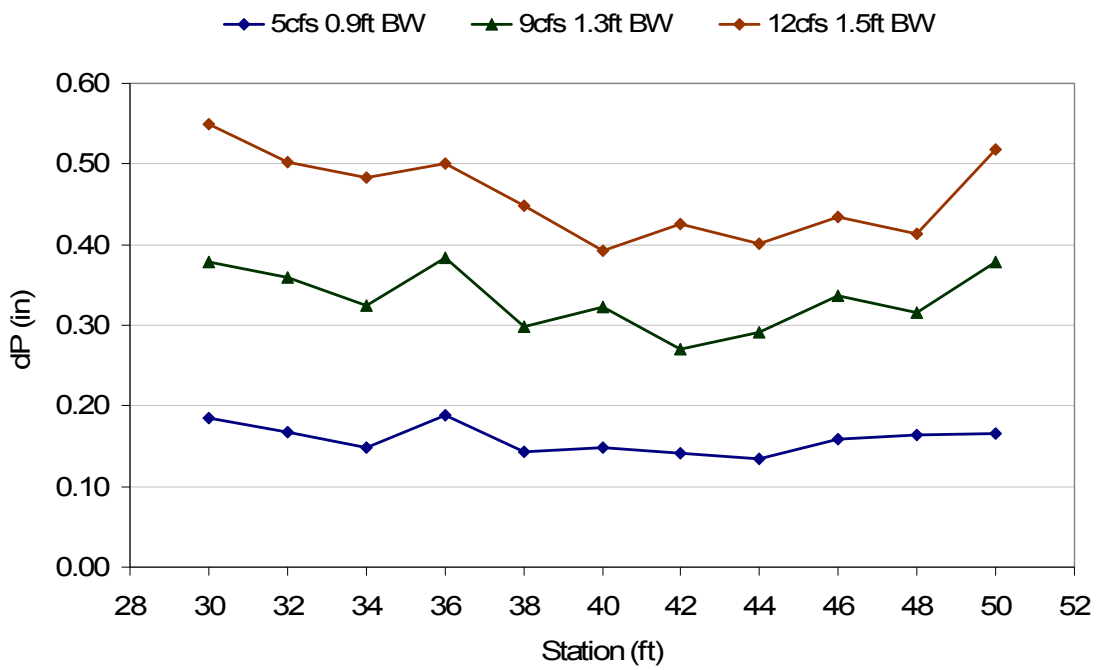

Figure 6.12: Concrete cap Preston tube measurements with normal depth backwater conditions.

\

7 ANALYSIS

For all of the tests in Figure 5.1, the Preston tube data was collected with corresponding shear stress computations. It was clear from reviewing Preston tube data for the gravel bed and concrete cap, that the two bed surfaces would need separate analyses along with separate calibration equations. For the gravel bed and concrete cap analyses, some of the outlier points were removed from the regression equations due to irregularities in bed form due to construction methods or irregular fluctuations due to transitions at the upstream and downstream boundaries. With the Preston tube, where differential pressure depended on the incompressible nature of water, air pockets in the plastic hoses leading from the Preston tube to the transducer, or in the transducer itself could have potentially caused erroneous results in the Preston tube readings. Every effort to eliminate air pockets was taken, including bleeding the lines before the tests for an extended period of time and keeping the lines bleeding while collecting depth data. While care was taken at every step of the construction and testing to facilitate uniform flow and accuracy in testing, some degree of spread was noted on the final Preston tube calibration curves.

Plotting the Preston tube measurements with the computed shear stress for the gravel bed, a regression line was fit with an r-squared value of .9804. Comparing the slope of the regression line for the 4-flume of 0.2986 to the slope of the Preston tube calibration on the 8-inch flume of 0.2804, the results appear to be reasonably consistent for similar

roughnesses. Figure 7.1 shows the regression of the gravel bed calibration data for the 4-foot flume.

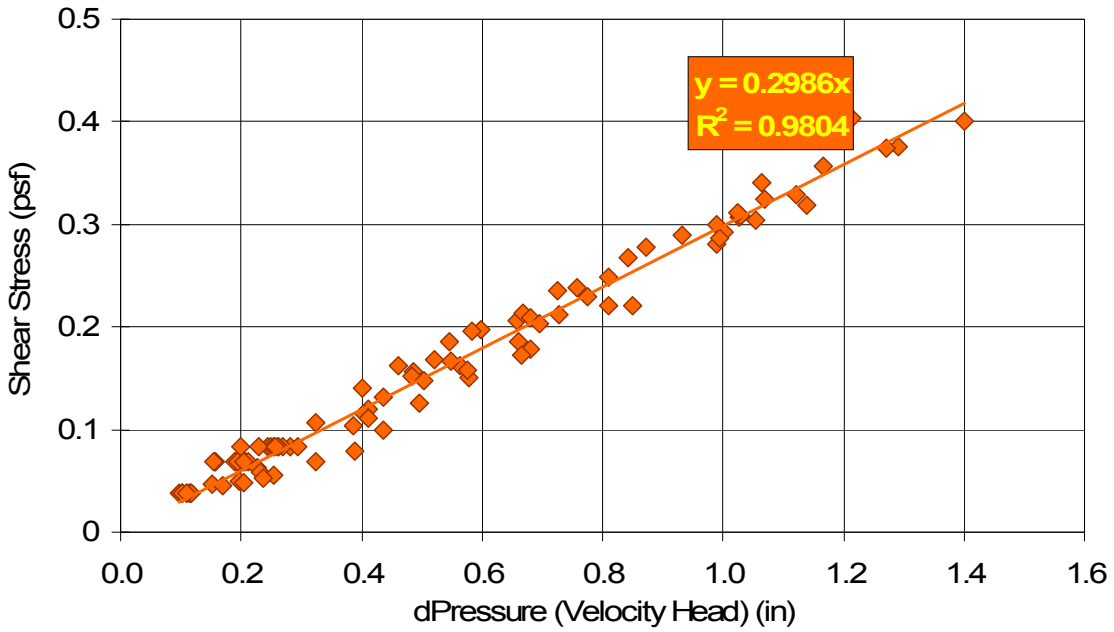

Figure 7.1: Preston tube calibration results in the 4-foot flume for the gravel bed.

Computed shear stress was plotted with Preston tube measurements for the concrete cap resulting in a regression r-squared value of .9747. A plot of the shear stress data versus the Preston tube data for the concrete cap is presented in Figure 7.2.

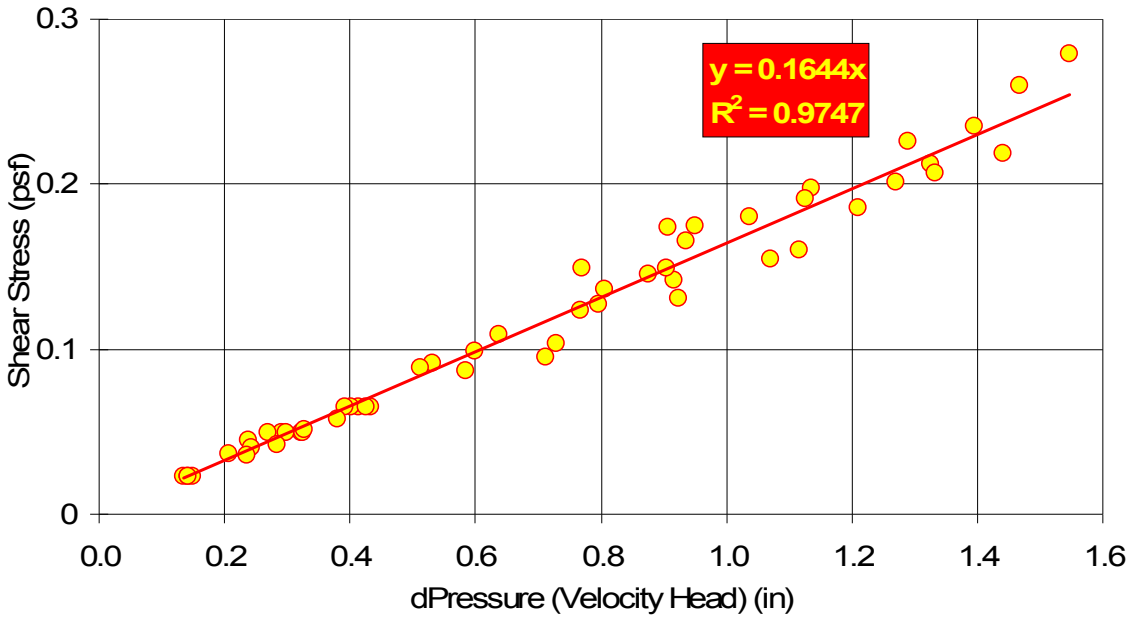

Figure 7.2: Preston tube calibration results in the 4-foot flume for the concrete cap.

A lower slope in the concrete cap calibration, 0.1644, is attributed to a reduced boundary roughness for the concrete cap. Validating results for the Preston tube calibration was done by comparing calibration curves from all the relevant sources found in the literature review, including Ippen and Drinker (1960), Heinz (2002), Preston tube calibration in the 8-inch, and calibration equations from the 4-foot flume. Figure 7.3 shows a comparison between Preston tube calibration equations obtained from relevant sources in the literature review.

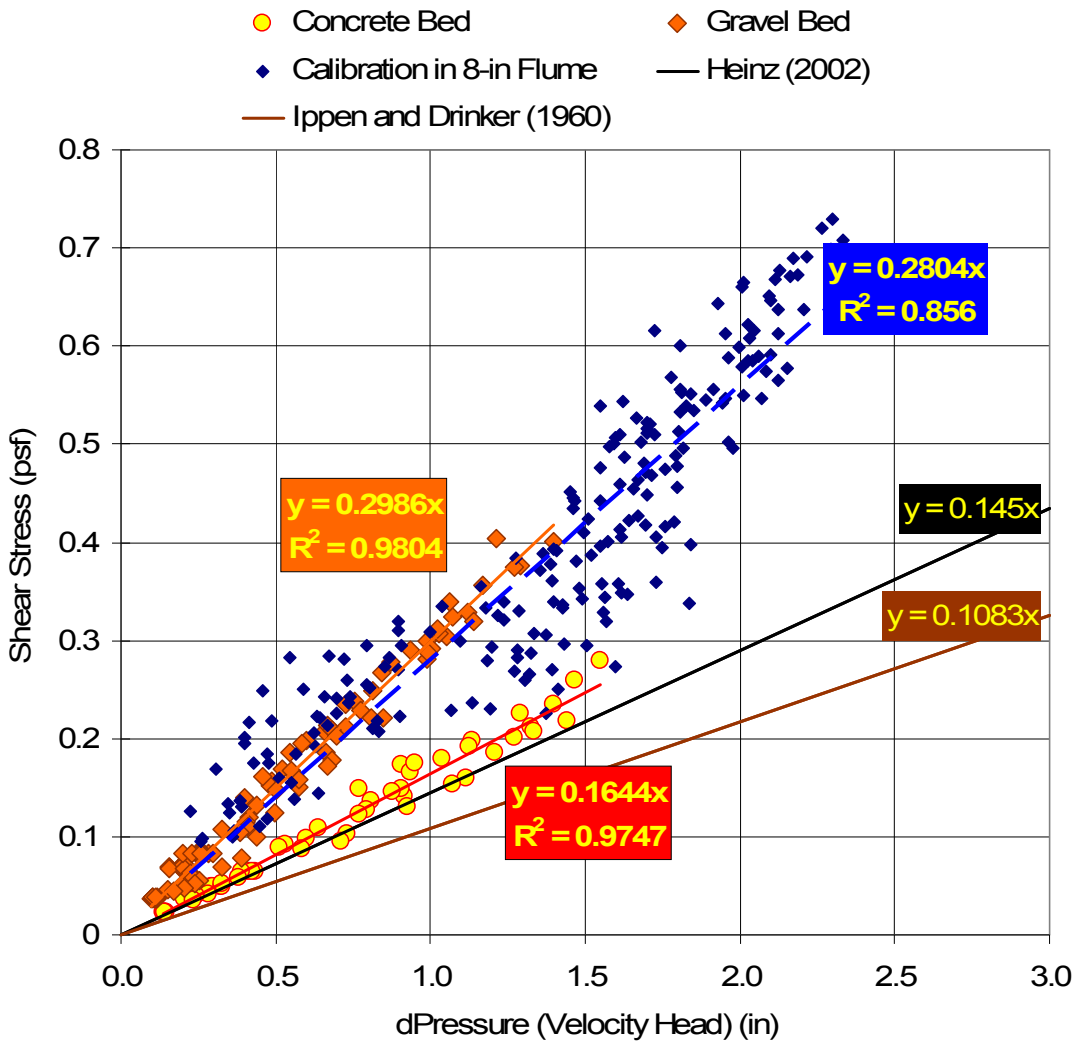

Figure 7.3: Preston tube calibration comparison

Figure 7.3 shows a close correlation between the calibration curve found in the 8-inch and the calibration curve found on the gravel bed in the 4-foot. Close correlation is shown in Figure 7.3 between Heinz (2002) and the results on the concrete cap in the 4-foot flume. From the data shown in Figure 7.3 it appears that boundary roughness has significant impact on the slope of the calibration equation used for the Preston tube. Accuracy in computation of the boundary shear stress, which is dependant on the

boundary roughness, is imperative for adequate Preston tube calibration results. Since Preston tube calibration equations developed for the gravel bed and the concrete cap reasonably match previous work, have well fitting regression lines, and are supported by data with adequate upper and lower limits, the calibration equations shown in Figure 7.3 are adequate for use in the Middle Rio Grande research.

8 CONCLUSIONS

In 1950 Ludwieg and Tillmann published a study that suggested a linear relationship exists between velocity profiles in a pipe and the boundary shear stress. Preston (1954) used Ludwieg and Tillann's 1950 study to establish empirical relationships between boundary shear stress and near boundary velocity. Hsu (1955) further validated Preston's 1954 work by analytically proving a relationship between the velocity profile and the boundary shear stress. Preston's 1954 study involved measuring the total pressure at the boundary with a pitot tube and the static pressure at the same locations using pressure taps in the pipe used in the tests. Later studies combined the measurement of the static pressure and the total pressure into one instrument, called the Preston tube, and applied it to open channel flow. Using a Preston tube, Ippen and Drinker (1960) established a linear realationship between near bed velocity and boundary shear stress for rough boundaries in open channel hydraulics along bends.

Heinz, 2002 used data from the CSU Middle Rio Grande model to develop a relationship for the Preston tube unique to the model's bend and bed roughness. Because Heinz (2002) used data located within a bend for calibration of the Preston tube, flow might not have been fully developed in a one-dimensional nature as originally suggested to be necessary by Preston (1954). To eliminate the effects of bend hydraulics, calibration of the Preston tube was performed using a straight 8-inch flume, with boundary conditions similar to the Middle Rio Grande model. Final calibration results

from the study in the 8-inch flume revealed a large spread around the mean calibration line. The large spread from the calibration in the 8-inch flume was thought to be the result of flow not being fully developed, either because the flume was too narrow, the upstream transition was too short, or the test section was not long enough.

The Preston tube was, again, calibrated in a 60-foot long, 4-foot wide, 2.5-foot tall flume with enough entrance transition, wave suppression, and dissipation to ensure fully developed flow. Calibration of the Preston tube in the 4-foot flume involved two bed materials, a ¼-inch gravel bed (which was mixed with cement with a 5 bags cement:1 ton gravel ratio) and a brushed concrete cap (mixed at a 2:1 ratio). After a 25-foot entrance section, depth and Preston tube data were collected in the center of the flume every two feet for 20 feet. Preston tube data was collected over a one (1) minute interval at a rate of 50 Hz and averaged over the minute before being used in calibration. Tests ranged from 2 cfs to 22 cfs with no backwater and from 5 cfs to 15 cfs with the backwater set at normal depth. A normalized profile was computed using standard step backwater procedures using a Manning's roughness that minimized the sum of the square errors between the measured profiles and the computed profile. From the normalized profile, momentum principles were utilized to determine the shear stress. Computed shear stress values were plotted against the average Preston tube measurements for each surface condition, gravel bed and concrete cap.

Two distinct calibration equations were developed for the Preston tube, one for the gravel bed and one for the concrete cap. Preston tube calibration equations develop from tests in the 4-foot flume for the gravel bed and the concrete cap are presented in Equation 8.1 and Equation 8.2, respectively.

$$\tau_o\,(\text{gravel bed}) = 0.2986 dP \qquad \textbf{Equation 8.1}$$

where,

τ_o = boundary shear stress (psf); and

dP = Preston tube measurement (differential pressure) (inches).

$$\tau_o(\text{concrete cap}) = 0.1644 dP \qquad \textbf{Equation 8.2}$$

where,

τ_o = boundary shear stress (psf); and

dP = Preston tube measurement (differential pressure) (inches).

From data gathered in the 4-foot flume and from Figure 7.3 it was evident that the relationship between the Preston tube measurement and boundary shear stress is related to surface roughness. As the roughness is increased, the slope of the calibration was found to be steeper. While tests performed in the 4-foot flume were tailored for the Middle Rio Grande model at CSU, the calibration equations could be applied, in general, to channel surfaces with similar boundary roughness. Further research could expand on the tests performed in this research by developing calibration equations for a range of roughnesses that are likely to be found in the laboratory setting. Application of the Preston tube in various natural settings would require calibration for each boundary roughness experienced.

While collecting Preston tube data is relatively simple, the need for calibration does complicate its use. Computed boundary shear directly from a complete velocity profile is possible and might negate the need for additional calibration. Comparing shear stress values computed from velocity profiles and shear stress computed from momentum principles or even previously calibrated Preston tube data might provide insight into alternative ways to measure boundary shear stress.

9 REFERENCES

Chow, Ven Te. Open Channel Hydraulics. New York: McGraw-Hill, 1959

Hsu, E.Y. (1955). "The Measurement of Local Turbulent Skin Friction by Means of Surface Pitot Tubes." David W. Taylor Model Basin, Report No. 957, August.

Heinz, M. (2002) Investigation of Bendway Weir Spacing. Master's Thesis, Colorado State University, Department of Civil and Environmental Engineering, Fort Collins, CO.

Ippen, A.T., Drinker, P.A., Jobin, W.R., and Noutsopoulos, G.K. (1960). "The Distribution of Boundary Shear Stresses in Curved Trapezoidal Channels." Department of Civil and Sanitary Engineering, Massachusetts Institute of Technology, Technical Report No. 43, October.

Ludweig, H., and Tillman, W. (1950) Investigations of the Wall-Shearing Stress in Turbulent Boundary Layers. National Advisory Committee for Aeronautics, Technical Memorandum 1285, May.

Munson, Bruce R., at. al. Fundamentals of Fluid Mechanics, 2nd Edition. New York: John Wiley and Sons, 1994.

Preston, J. H. (1954) "The Determination of Turbulent Skin Friction by Means of Pitot Tubes." *Journal of the Toyal Aeronautical Society*, Vol. 58: 109-121.

Rouse, Hunter. (1946). Elementary Fluid Mechanics. New York: Dover Publications, Inc..

Rosemount. (2002) Annubar Flowmeter Series Reference Manual. Rosemount, 00809-0100-4809, August.